ELECTRICAL CHARACTERISTICS OF THERMALLY GROWN Al_2O_3 FILMS

A Thesis Submitted
in Partial Fulfilment of the Requirements
for the Degree of

MASTER OF TECHNOLOGY

by

L. VIJAYRAGHAVAN

to the

MATERIALS SCIENCE PROGRAMME
INDIAN INSTITUTE OF TECHNOLOGY KANPUR
February, 1990

CERTIFICATE

This is to certify that the research work contained in the M.Tech thesis entitled "ELECTRICAL CHARACTERISTICS OF THERMALLY GROWN Al_2O_3 FILMS" by Mr.Vijayaraghavan L. has been carried out under my supervision and that the same has not been submitted elsewhere for a degree.

Jitendra Kumar

January, 1990

(Jitendra Kumar)
Professor
Materials Science Programme
Indian Institute of Technology
Kanpur

ACKNOWLEDGEMENT

I derive esteemed pleasure in expressing my sincere gratitude to Dr.Jitendra Kumar for his invaluable guidance and cooperation during the course of this investigation.

I would like to thank Mr.Seshadri, Mr.Sanjay Kumar, Ms. Anu Gupta, Mr.Dharampal Goel, Mr.Padmanabhan for their valuable contribution towards the completion of my thesis.

Thanks are due to my friends Barik , Ravi, Gogate, Subash, Hamid and others for giving a finishing touch to my thesis.

Finally, I would like to thank all my friends in hall four for their constant encouragement throughout the duration of my stay in the campus.

I am also grateful to my family for providing me with such an oppurtunity and for the love and affection bestowed on me.

(VIJAYARAGHAVAN L.)

TABLE OF CONTENTS

LIST OF FIGURES

Fig.3.2 Current-Voltage characteristics of the Al-Al_2O_3-Al structure for insulator thickness (a) 3.8nm (b) 4.4nm (c) 4.9nm (d) 5.7nm

Fig.3.3 Log I - Log V characteristics of the Al-Al_2O_3-Al structure for insulator thickness (a) 3.8nm (b) 4.4nm (c) 4.9nm (d) 5.7nm

Fig.3.4 Ln I - $V^{\frac{1}{2}}$ characteristics of Al-Al_2O_3 structure for insulator thickness (a)3.8nm (b)4.4nm (c)4.9nm (d)5.7nm

Fig.3.5 Log(I/V) - $V^{\frac{1}{2}}$ plots of Al-Al_2O_3-Al structure for insulator thickness (a) 3.8nm (b) 4.4nm (c) 4.9nm (d) 5.7nm

Fig.3.6 Ln(I/V^2) - 1/V plots of Al-Al_2O_3-Al structure for insulator thickness (a)3.8nm (b)4.4nm (c)4.9nm (d)5.7nm

Fig.3.7 Voltage (V) - thickness (t A°) curves for Al-Al_2O_3-Al structure at constant current (a)20 nA (b) 40 nA (c) 80 nA (d) 120 nA (e) 140 nA

Fig.3.8 I - V characteristics for Al-Al_2O_3-Al structure taken initially and after 24 hours for insulator thickness (a) 3.8nm (b) 4.4nm (c) 4.9nm (d) 5.7nm

Fig.3.9 I - V characteristics for Al-Al_2O_3-Al structure in categories b and c for insulator thickness (a) 3.8nm (b) 4.4nm (c) 4.9nm (d) 5.7nm

Fig.3.10 I - V characteristics of an 3.6nm thick Al_2O_3 film with (a) base negative (b) base positive

Fig.3.11 Idealised trapezoidal potential barrier showing barrier shapes in Al-Al_2O_3-Al structures (a) unbiased (b) base aluminium electrode negatively biased (c) base aluminium electrode positively biased

List of tables

Name : Vijayaraghavan L.

Roll No. : 8721206

Programme : M. Tech. / Materials Science

Thesis Title : Electrical Characteristics Of Thermall Grown Al_2O_3 Films

Thesis Supervisor : Dr. Jitendra Kumar

ABSTRACT

The studies relating to the electrical characteristics of insulating films have received considerable attention in recent past from both fundamental and application view points. This has happened primarily because thin insulating films show useful properties and have found immense application in switching, memory and emission devices. Of particular interest is thin aluminium oxide films. An attempt has been made in the present study to investigate its electrical characteristics. Metal -insulator - metal structures have been prepared by deposition of aluminium films in a vacuum of 10^{-5} torr and oxidising them upto certain depth in air or oxygen for 24 hours at 50, 100 and 150°C and then depositing cross aluminium films over them. The thickness of the dielectric (Al_2O_3)has been determined by capacitance measurement taking due account of the interfacial contribution. The current - voltage data have been analyzed using I - V ,logI - logV, lnI - $V^{½}$, $\ln(I/V^2)$ - 1/V, and $\ln(I/V)$ - $V^{½}$ plots to show ohmic behaviour, Schottky emission and thermal field emission mechanisms operating simultaneously. It is further observed that the barrier height in the Schottky emission regime takes reduced value in comparison to the theoretical estimated value

and increases with increase in dielectric thickness. This reduction has been attributed to the lowering of potential barrier due to the image forces. 'Forming' process, involving a perceptible change in the dielectric properties, followed by appearance of the voltage controlled negative resistance (VCNR) have been observed in thermally grown Al_2O_3 films for the first time. 'Forming' potential is found to be around 10 volts for all the dielectric thicknesses. The emergence of conducting channels in thermally grown Al_2O_3 and their rupture are shown to be responsible for the 'Forming' and VCNR, respectively. Dielectric breakdown occurs in these films beyond the VCNR regime. However,no forming process is observed in thin Al_2O_3 layers (< 5 nm). These devices show a continuous rise in current with applied voltage leading to its breakdown eventually. The emergence of discontinuities in conducting filamentary channels, possible loss of electrode - oxide contact and/or total destruction of oxide layer appear(s) to be responsible for the dielectric breakdown of Al - Al_2O_3 - Al junctions. Though Al - Al_2O_3 - Al junctions are symmetric in construction, their current - voltage characteristics are asymmetric in nature. This asymmetry is explained on the basis of a graded type barrier at the interface between the bottom electrode and oxide and an abrupt type at the interface between the oxide and the top electrode.

CHAPTER 1

INTRODUCTION

Rapid progress in electronic microminiaturisation during the last two decades owes its success to a great extent to the development of thin film devices which have advantages of space, weight, power saving, in addition to reliability, rugged construction, flexibility of design, low maintenance and low cost. Most of these devices work basically on the passage of current through thin layers of poorly conducting materials and/or semiconductors. As a consequence, immense interest has aroused in the studies of electrical conduction in thin films of various materials. Of particular interest are thin insulating films like SiO [1], SiO_2 [2], Al_2O_3 [3-7], TiO_2 [8-9], Ta_2O_5 [10] etc. The present thesis also deals with the electrical characteristics of thin alumina (Al_2O_3) films.

Above absolute zero, conduction in insulators can take place due to thermal excitation of electrons and may be influenced by structural defects and impurities present. There are several conduction mechanisms (shown schematically in Fig.1.1) reported to be operating in thin insulating films [11-12]. An electron donated by the impurity species in the insulator will have its wave function localised about the impurity. Since there is a small but finite overlap of wavefunctions of donor electrons, there can be hopping from one trapping/impurity centre to another without going up into the conduction band. This is termed as impurity conduction [13-14]. There will therefore be appreciable rise in current flow if there are sufficient impurity centres. At high temperatures, point defects allow net movement of ions under the influence of

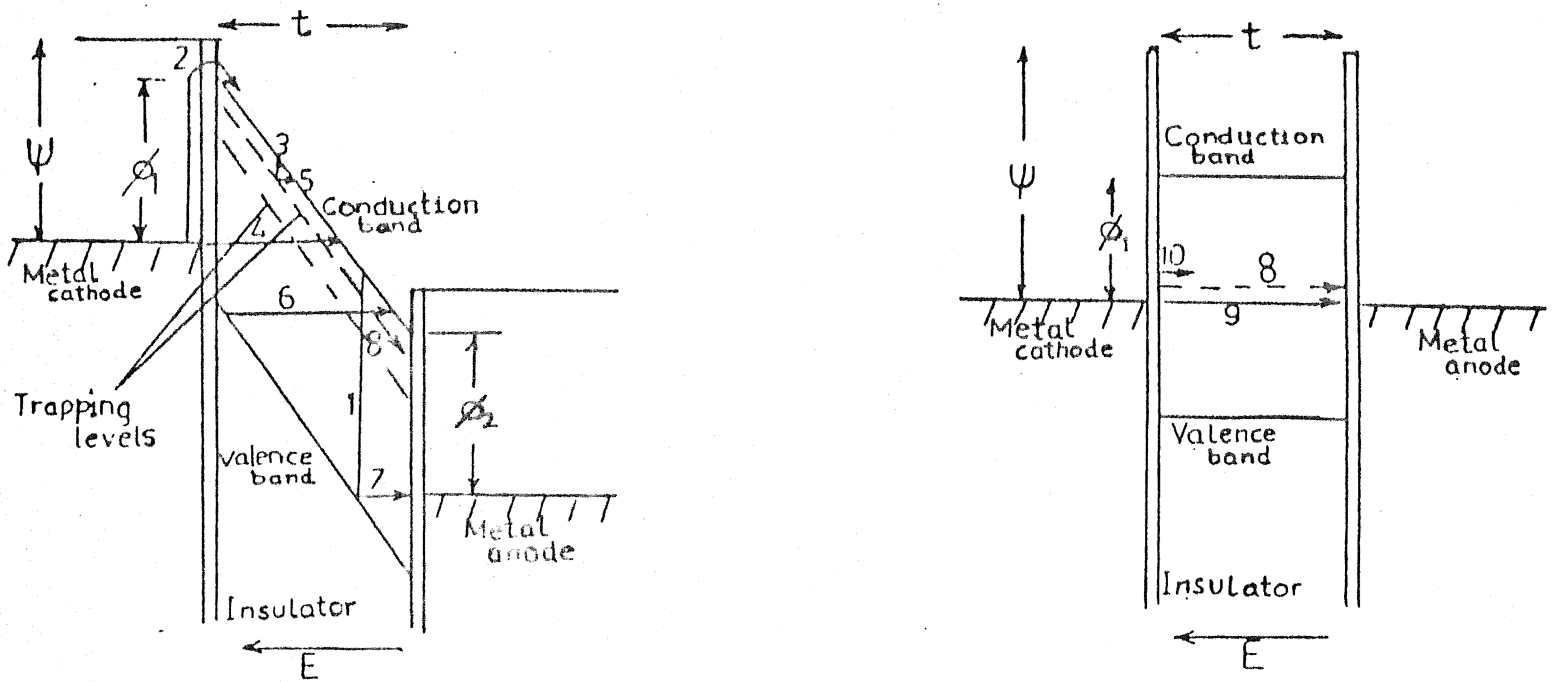

Fig.1.1 Schematic diagram of various conduction processes in thin dielectric films

1. Electrons raised thermally from valence band if band gap is small & temperature is high
2. Schottky emission from the metal
3. Thermal excitation into the conduction band from trap levels in the insulators
4. Tunneling from metal into the conduction band
5. Tunneling from trap levels in the insulator
6. Tunneling directly from valence band to conduction band
7. Tunneling from valence band of insulator into metal electrode directly
8. Ionic conduction
9. Tunneling directly between two metal electrodes
10. Impurity conduction

electric field and so ionic conduction is said to occur [11-12]. The characteristics of ionic current are large activation energy, increase of resistivity with time at constant d.c. voltage (perhaps due to the space charge accumulation i.e. polarisation), transport of material from one electrode to another, and large transit time for ions [15]. Under ambient conditions, ionic current is negligible and so the current that flows is essentially electronic in nature. Three main processes that contribute to the electronic current in thin insulating films are (i) tunneling (ii) Schottky-emission and Poole-Frenkel effect, and (iii) space-charge limited effects.

1.1 Tunneling

When an insulator is placed in the gap between two similar metal electrodes the potential barrier is lowered [16] by an amount $\psi - \phi_o$ where ψ (the distance between the fermi level and vacuum level) is known as work function of the metal and ϕ_o is the distance between the bottom of the insulator conduction band and the fermi level of the metal electrodes (Fig 1.2a & 1.2b). The probability that an electron can penetrate a potential barrier is a function of its energy, size and shape of the barrier. On applying an electric field, electrons occupying states in one metal electrode can tunnel through the insulator into the empty states on the other side. This is so because electrons of negatively biased electrodes 'see' a potential barrier smaller in height by amount eV in comparison to the other side. Consequently, tunneling results with a net electronic current flow from negative to positively biased electrode (Fig. 1.2c).The current density is found to depend on the barrier shape, image forces, space charges and traps.

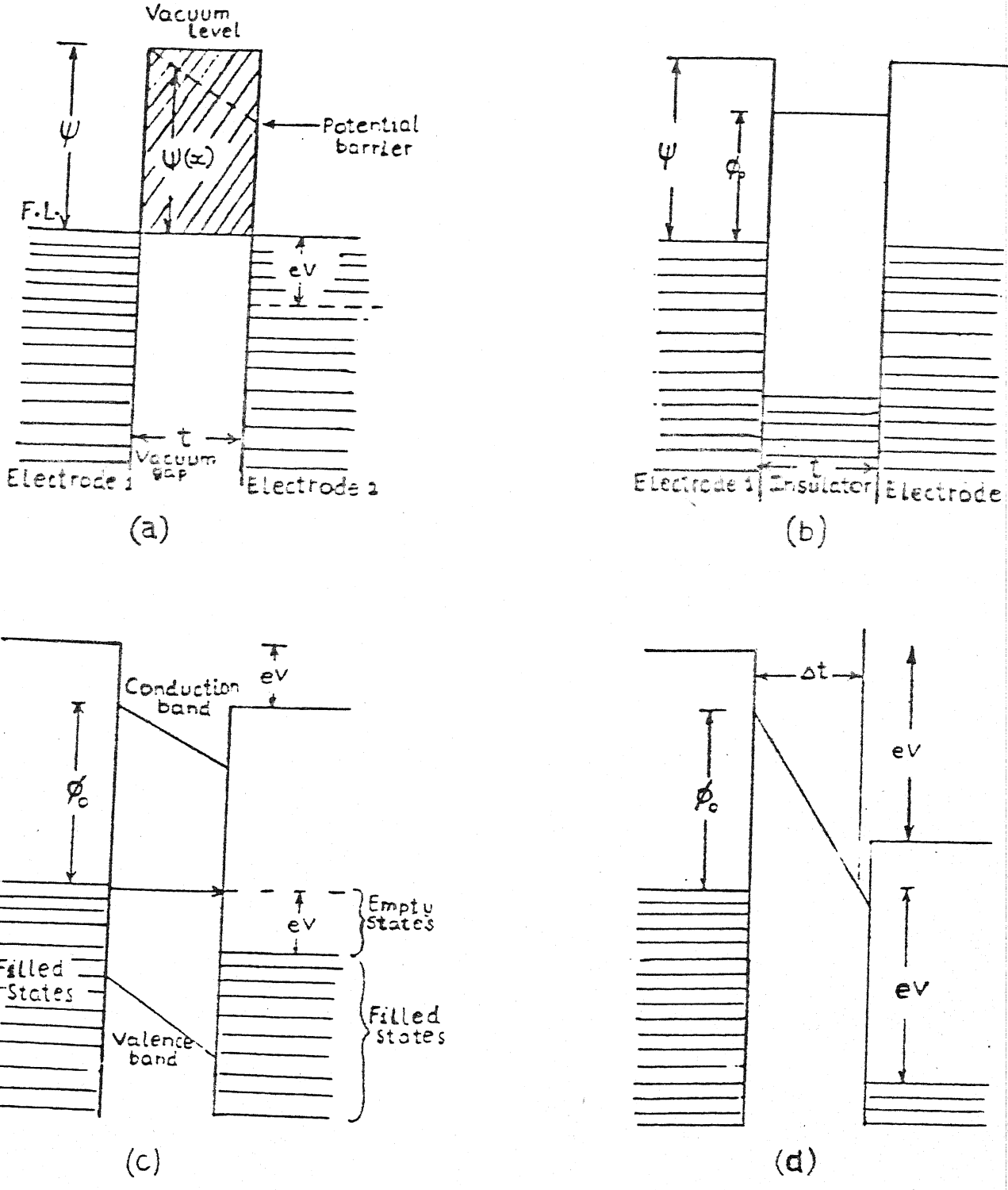

Fig 1.2 Potential energy band diagram for (a) metal-vacuum metal and for metal-insulator-metal with rectangular barrier for (b) V=0 (c) $V<\phi_o/e$ (d) $V>\phi_o/e$

Simmons [17] using WKB approximation for a generalised barrier with similar electrodes found the relation for the current density as

$$J = J_o(\bar{\phi}\exp(-A\bar{\phi}^{1/2}) - (\bar{\phi}+eV)\exp[-A(\bar{\phi}+eV)^{1/2}]) \quad \ldots.(1)$$

Where $J_o = \dfrac{e}{2\pi h(\Delta t)^2}$, $t = t_2 - t_1$, $A = \dfrac{4\pi\Delta t(2m)^{1/2}}{h}$

t_1, t_2 are limits of barrier at the fermi level, $\bar{\phi}$ is effective barrier height, e is electronic charge, h is the Plancks constant, and m is electron mass. Equation (1) can be interpreted as current density $J_o\ \bar{\phi}\exp(-A\bar{\phi}^{1/2})$ from electrode 1 to electrode 2 and a current density $J_o(\bar{\phi}+eV)\exp[-A(\bar{\phi}+eV)^{1/2}]$ from electrode 2 to electrode 1, resulting in the net current density J. For a rectangular barrier, relation (1) leads to the following dependences:

For $V \approx 0$

$$J = \text{constant} \cdot V \quad \ldots.(2)$$

The constant involves barrier height and insulator thickness. This relation shows ohmic conduction. For $0 < v < \phi$, J is a non linear function of V, such that,

$$J = B\ V \exp[-B'\ V^{1/2}] \quad \ldots.(3)$$

Here, B and B' are constants.

For very high applied voltages the Fowler - Nordheim equation for field emission results i.e.

$$J = C\ V^2 \exp -\left(\frac{\alpha}{V}\right) \quad \ldots.(4)$$

Where C and α are constants involving barrier height and insulator thickness (Fig. 1.2d).

The energy band diagrams as shown in Fig 1.2 (a,b,c,d) with abrupt changes in potential are physically unrealistic. In fact the potential step changes smoothly as a result of the image forces.

This arises due to the metal surface becoming positively charged as an electron escapes. The positive charge, in turn, exerts an attractive force on the escaping electron. The effect of the image force is to change the size and shape of the potential barrier by rounding off the corners (i.e. reducing the height of the barrier from ϕ_o to ϕ') and also reducing the thickness of the barrier (Fig.1.3). Thus the current density relation [equation (3)] takes the form

$$J = J_o \{\phi' \exp(-A\phi'^{\frac{1}{2}}) - (\phi'+ev)\exp[-A(\phi'+ev)^{\frac{1}{2}}]\} \quad ....(5)$$

The current voltage relationship has the similar behaviour as for the rectangular barrier case, except, that the barrier height has now changed from ϕ_o to ϕ' where

$$\phi' = \phi_o - \alpha' V - D' \quad ....(6)$$

where α' and D' are constants involving insulator thickness and ϕ_o is height of the rectangular barrier (Fig.1.4) Due to accumulation of electrons in the conduction band, space charge is created and potential rises at the centre of the insulator. For very thin insulating films and for the maximum potential value (ϕ_m) at centre of the insulator greater than kT, the space charge effect is found to be negligible [18]. However, if traps are present space charge effects tend to reduce tunnel current considerably. In addition, the very presence of traps, delays and limits the electrons in crossing the barrier for a finite lifetime of the traps [9]. When a trap is occupied, it cannot capture electrons and so enhancement of current is noticed which exhibit temperature dependence.

The tunneling of electrons through insulating films sandwiched between metals was first considered by Frenkel [1]. He derived approximate results for linear and quadratic voltage terms in the

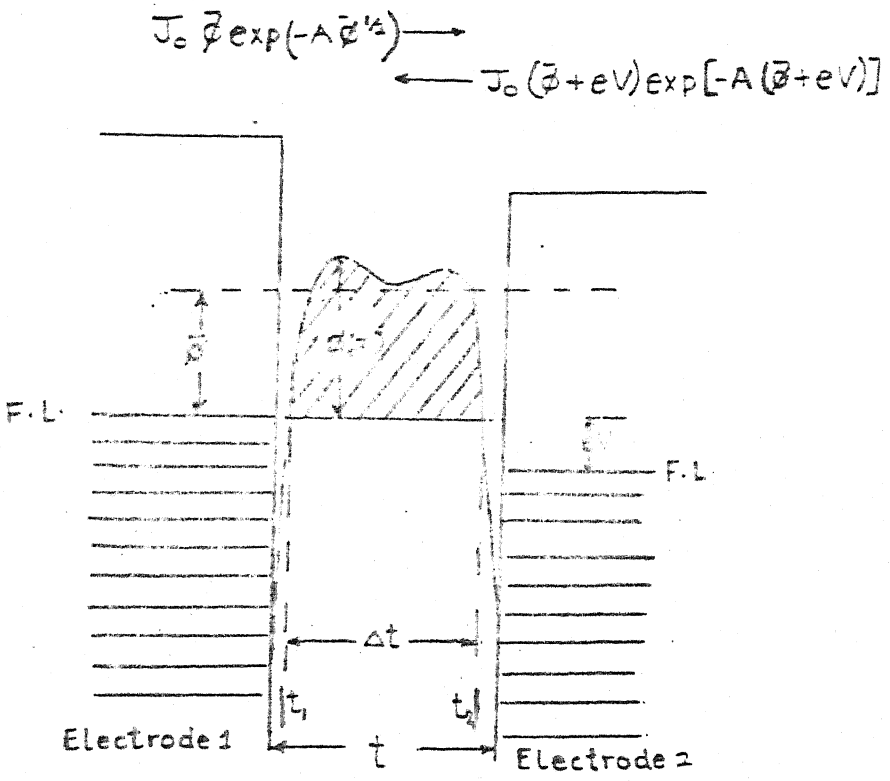

Fig 1.3 Schematic diagram showing current flow between the electrodes for a generalised barrier

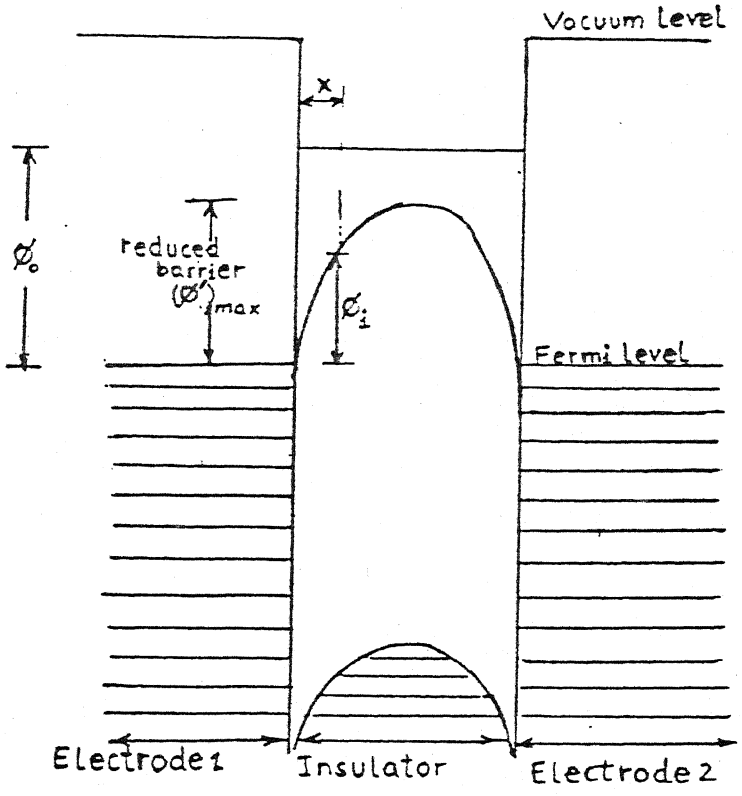

Fig 1.4 Effect of image force on a symmetric barrier

voltage-current characteristics at absolute zero, taking into account rectangular potential barrier. Tunneling effect in thin insulators was also studied by Holm [3] neglecting the effect of image forces and using a symmetric parabola-approximation for the barrier. A generalised expression for tunneling through a potential barrier of arbitrary shape with and without the consideration of image forces was given by Simmons [17] as well. This expression in conjunction with low voltage characteristics obtained by Holm show that the parabolic approximation is good for high barriers but inadequate for low barriers. Simmons further observed that smaller the value of dielectric constant, lower is the tunnel resistivity. Later on, Simmons [19] extended his theory to asymmetric junctions and estimated the intrinsic field present in them for Al-Al_2O_3-Au and Al-Al_2O_3-Sn systems. The passage of current through Al-Al_2O_3-metal structures was investigated by Pollack and Morris [20] to show that the trapezoidal energy barrier model of Simmons [19] adequately accounts for the observed current - voltage characteristics. Handy [21] reported that the asymmetric junction resistance increases with increase in size of atomic radius of counter electrode metal till 1.6 A and then levels off. This can be explained on the basis of penetration of the metal atoms into the oxide and reducing thereby the barrier thickness. The observed electrical asymmetry in Al-Al_2O_3-Al system is attributed to the difference in surface states at the two interfaces [19]. Gundlach [22] used the two band model to explain the characteristic features of tunneling such as maxima in the logarithmic derivative curves, maxima in thermal I-V characteristics and zero bias offset of the conductance minimum. Gundlach and Holzl [23] have determined barrier parameters using trapezoidal barrier shape for plasma

and thermally oxidised Al-Al_2O_3-Al junctions and their logarithmic derivative characteristics. The values of barrier height obtained by them from the position of logarithmic conductivity maxima were in good agreement with those found from photoelectric measurements. Kumagai, Inukai and Suzuki [24] attributed the discrepancy between theoretical and experimental values of tunneling current to the non-uniformity of thickness of oxide layer in Al-Al_2O_3-Al. They expressed the non-uniformity of thickness by a modified Poissons distribution function. Geppert [18], Wintle [25], Gupta and Overstraeten [26] have studied the role of trap states in the dielectric region on the metal-insulator-metal characteristics. Srivastava, Roy Bardhan and Bhattacharya [27] have introduced traps by neutron irradiation of the Al-Al_2O_3-Au junctions and found enhancement of current, with junction resistances decreasing by three orders of magnitude. They further pointed out that vacancies might also act as traps. Sarnot and Dubey [28] derived the current - voltage characteristics for a metal-insulator-metal structure with an arbitary barrier taking into account a non-parabolic E-K relation. They found that the non-parabolic band structure affects the tunnel current by 2-3 orders of magnitude and invariably (except for the temperature dependence of tunnel current) provides a better correlation between theory and experiment. Giaver and Fisher [29], Giaver and Megerle [30] have found that the linear feature of the tunneling current for Al-Al_2O_3-Pb becomes non-linear in character when one metal is in superconducting state. For both metals in the superconductive state, even a negative resistance region is obtained. Fisher [29] used the current-voltage characteristics to determine energy gap of metals for Al-Al_2O_3-metal systems. The variation in energy gap

width with temperature agrees closely with the BCS theory.The energy gap can be decreased by increasing the magnetic field around the junction. Blackford and March [31], Douglass and Meservy [32] obtained the superconducting energy gap for Al-Al_2O_3-Pb structure and noticed the existence of a negative resistance in agreement with the BCS theory. Glaver, Hart and Megerle [33] observed tunneling into superconductors like lead, tin, indium, aluminium below 1° K for Al-Al_2O_3-metal systems and obtained the values of density of states for these metals.

1.2 Schottky emission

Due to the high fields obtainable across thin insulating films, the potential barrier is effectively reduced with the result that electrons possessing energy greater than this barrier may escape into conduction band of the insulator. This is known as Schottky emission effect [Fig.1.5]. Consider an electron a distance x from the surface of an uncharged metal. The only force on electron is the classical image force [12,19,34], $e^2/4\pi\epsilon_o K^* x^2$ which is attractive in nature. Therefore the potential energy of the electron due to image force becomes

$$\phi_{im} = - \frac{e^2}{16\pi\epsilon_o K^* x} \qquad \ldots.(7)$$

Where e is electronic charge, ϵ_o is permittivity of free space, K^* is the high frequency dielectric constant. The potential step (with respect to the Fermi level) taking into account the image potential at a distance x from the interface is given by

$$\phi(x) = \phi_o + \phi_{im} = \phi_o - \frac{e^2}{16\pi\epsilon_o K^* x} \qquad \ldots.(8)$$

Where ϕ_o is rectangular potential barrier height. The barrier

$\phi(x)$ in presence of image forces is shown by curve AB in Fig.1.5. Schottky assumed that image force holds only for x greater than some critical distance x_o [34]. For $x < x_o$, potential energy is a linear function of x. When an electrical field exists at metal-insulator surface, it interacts with the image force and lowers the potential barrier. The line CD represents the potential due to a uniform field, which when added to the barrier potential $\phi(x)$ produces the potential step shown by dashed line [Fig.2.5].The net potential of the barrier $\phi(x)$ therefore becomes

$$\phi(x) = \phi_o - \frac{e^2}{16\pi K^* \epsilon_o x} - e E x \qquad \ldots.(9)$$

Where E is the applied field.

The effect of image potential is to reduce the area of the potential barrier between the electrodes by rounding off the corners and reducing the height and width of the barrier. The minimum change ($\Delta\phi$) in the barrier height (ϕ) can be given by

$$\Delta\phi = \left(\frac{e^3}{4\pi K^* \epsilon_o}\right)^{\frac{1}{2}} \cdot E^{\frac{1}{2}} = \beta_s E^{\frac{1}{2}} \qquad \ldots.(10)$$

Since the image force lower the barrier height, the current does not saturate in accordance with the Richardson law $J = AT^2 \exp(-\phi_o/kT)$. Instead , it is given by the Richardson-Schottky expression [34,19],

$$J = AT^2 \exp - \left(\frac{\phi_o - \Delta\phi}{kT}\right) \qquad \ldots.(11)$$

By substituting the value of $\Delta\phi$,

$$J = AT^2 \exp \frac{\phi_o}{kT} \exp \left(\frac{\beta_s V^{\frac{1}{2}}}{kT}\right) \qquad \ldots.(12)$$

Where $A = \frac{4\pi me(kT)^2}{h^2}$ is Richardson - Dushman constant

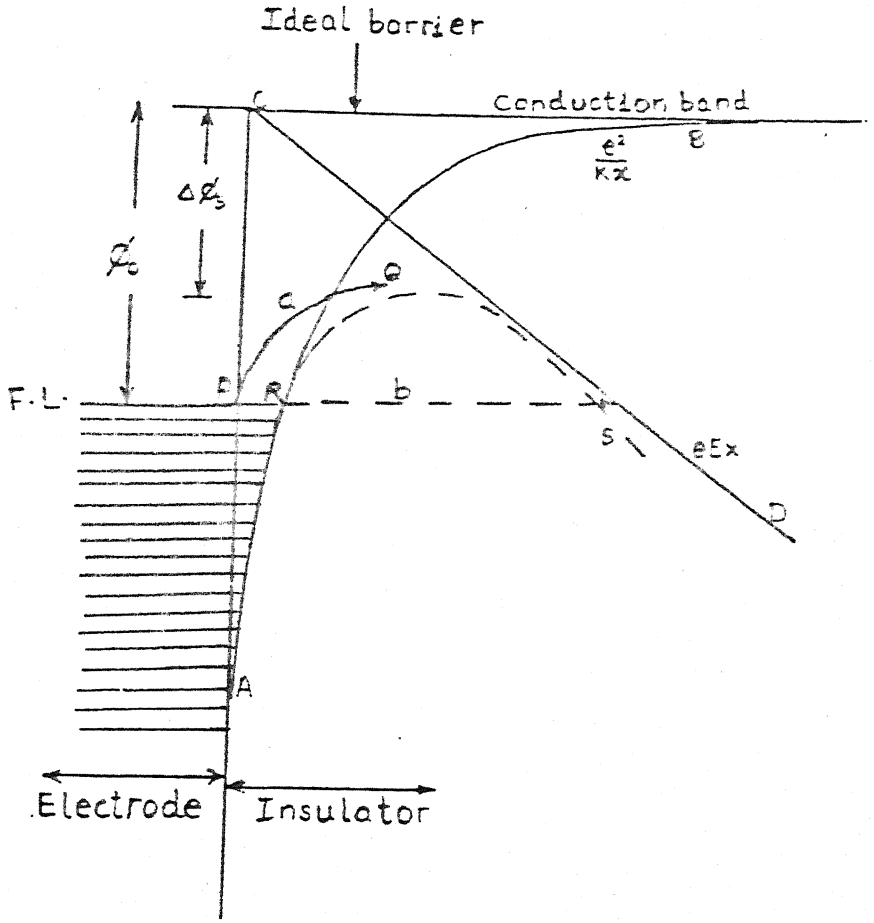

Fig 1.5 Schottky emission over the reduced barrier (curve PQ) and tunneling through the barrier (along RS)

in units of amp cm-2 °K-2 for J in A cm-2 and

$$\beta_s = \left(\frac{e^3}{4\pi K^* \epsilon_o t} \right)^{1/2}$$ is the Schottky conduction coefficient

in $(\text{volts})^{-1/2}$, where t stands for the thickness of the insulator. We see therefore from equation (12) that Schottky current unlike tunnel current is temperature dependent. The Richardson-Schottky effect was first observed by Emptage and Tantraporn [35] in 50 A° thick insulator of Al-Al_2O_3-Al. Accordingly a linear behaviour was found in the ln I versus $V^{1/2}$ plot. The barrier height determined from the intercept was Ø=0.74ev. Similar values of barrier height, i.e. 0.73ev and 0.97 were determined by other workers [7,36] providing evidence for Schottky emission. The low value of barrier height obtained in comparison to 1.6-2.34 eV reported [37-39] for tunneling was explained by Schmidt et al [40] to be due to the migration of oxygen vacancies under the influence ef the field resulting in the formation of positive space charge layer in the oxide film near the cathode Simmons [19] taking into account the effect of image forces on barrier shape studied the emission limited current flow between electrodes for symmetric and asymmetric junctions. Accordingly thermionic or tunnel current predominates depending on barrier height and applied voltage. Vodenicharov and Christov [41] have shown that metal-insulator work functions determined by thermionic emission gives reliable values and can be used as such for explaining the current-voltage characteristics of Al-Al_2O_3-Al junctions in all possible emission conditions viz : thermionic, field and therm onic-field emission. In doing so, they found fair agreement between the experimental results and the general theory of electron currents through dielectrics with a large energy gap. Since the thermal emission falls off rapidly with decreasing temperature, field emission can

only be responsible for conduction at low temperatures. Pollack [42] observed that the electrode limited conduction process change from Richardson-Schottky to the field-emission in both relatively thick and very thin insulators as the sample was cooled from room temperature to liquid nitrogen temperature.

1.3 Poole-Frenkel effect

The Poole-Frenkel (field assisted thermal ionization) effect is the lowering of a coulombic potential barrier when it interacts with an electric field and is usually associated with traps or donor centres in the bulk of an insulator (Fig.1.6) This is the bulk analog of the Schottky effect at an interfacial barrier and is applied to the thermal excitation of electrons from traps or donor centres into the conduction band of the insulator [12,43] The potential energy of an electron in a coulombic field is $-e^2/4\pi\epsilon_o K^* x$ where K^* is high frequency dielectric constant, ϵ_o is the permittivity of free space, x is distance in the insulator. This energy is four times to that resulting from the image force effects. This leads to lowering of the coulombic barrier in a uniform field such that

$$\phi_{pf} = \left(\frac{e^3}{\pi\epsilon_o K^* t}\right)^{\frac{1}{2}}, \quad V^{\frac{1}{2}} = \beta_{pf} V^{\frac{1}{2}} \qquad \ldots.(13)$$

Where $\beta_{pf} = 2\beta_s$

Mead [44] has given an expression for the Poole-Frenkel current density in thin film insulators containing shallow traps as

$$J = J_o \exp\left(\frac{\beta_{pf} V^{\frac{1}{2}}}{kT}\right) \qquad \ldots.(14)$$

In principle it should therefore be possible to differentiate between Poole-Frenkel and Schottky effect from the different

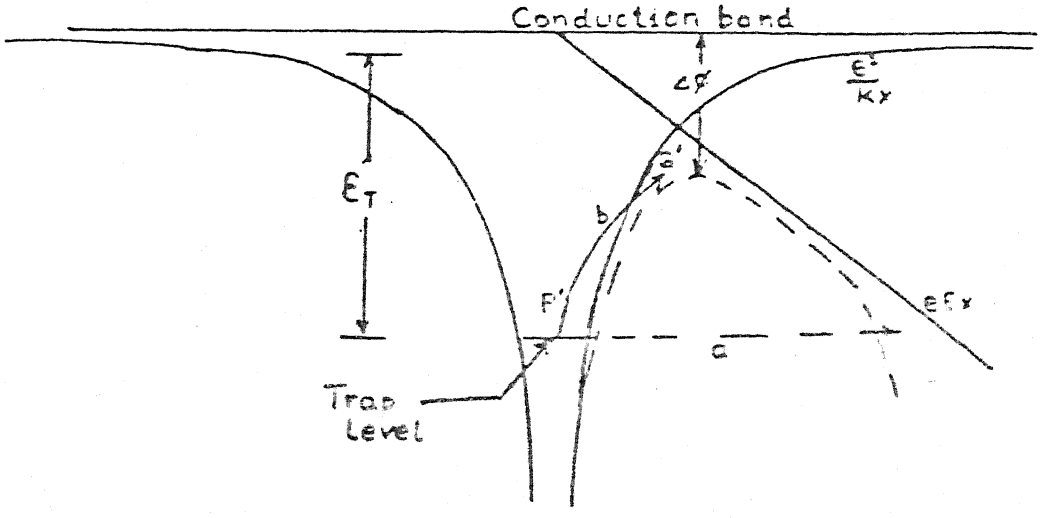

Fig 1.6 Poole-Frenkel current over reduced barrier(curve P'Q') and tunneling of electrons through the barrier (R'S')

dependence of conduction on field strength. A graph of ln I versus $V^{\frac{1}{2}}$ results in a straight line with slope β_s or β_{pf} depending on the mode of conduction. If one looks at the ln I versus $V^{\frac{1}{2}}$ and ln (I/V) versus $V^{\frac{1}{2}}$ Curves in conjunction and voltage range match for straight lines in both, Poole-Frenkel effect is considered to be responsible for the current as

$$I \alpha V \exp - \left(\frac{\phi_o - \beta V^{\frac{1}{2}}}{kT} \right) \quad \ldots.(15)$$

Where ϕ_o stands for the barrier associated with traps [47]. Also slopes of straight line regions of ln I versus $V^{\frac{1}{2}}$ curve are found out and plotted against (insulator thickness)$^{-\frac{1}{2}}$. This results in straight line, the slope of which can be used to distinguish between the two conduction processes, namely Schottky-emission and Poole-Frenkel effects [44,46,47]. While in case of former, slope value differ as the electrode material is altered, they remain essentially same in case of latter i.e. Poole-Frenkel effect [45]. β_s and β_{pf} can also be determined theoretically using the expression, $\beta = e^{3/2} (\pi t K^* \epsilon_o)^{\frac{1}{2}}$ [43,48-49] and compared with the experimental findings. Antula [50] doped thin insulating films with positive ions (Cd,Cu,Ni) or negative ions (I) and showed that schottky emission predominates for both doped and undoped samples for insulator thickness less than 10 nm and Poole-Frenkel effect becomes operative for thick films (say 40 nm). For intermediate thickness 20 nm doped and undoped samples exhibit Poole-Frenkel and Schottky emission, respectively. In order to explain the Poole-Frenkel effect Simmons [43] assumed that the insulator contains donor centres, which lie below the fermi level energetically and shallow neutral traps. The I-V characteristics therefore takes the

form

$$J = J_o \exp\left(\frac{\beta_{pf} V^{\frac{1}{2}}}{2kT}\right) \quad \ldots.(16)$$

This amounts to relation that is valid for Schottky emission also as $\beta_{pf} = 2\beta_s$. Therefore there turns out to be an anomaly in this situation where Poole-Frenkel conductivity (which is bulk limited) and current due to Schottky emission (said to be electrode limited) have the same dependence on applied voltage.

1.4 Space charge limited (SCL) currents

If an ohmic contact is made to the insulator, space charge is formed in conduction band of the insulation due to the electrons injected from the metal . This is capable of controlling current flow and this process is termed SCL conduction [18]. Mott and Gurney [51] obtained the SCL current voltage dependence for a trap free insulator of thickness t having no intrinsic carriers as

$$J \alpha \frac{V^2}{t^3} \quad \ldots.(17)$$

However, low current density than predicted by this relation are observed experimentally. Rose [52] worked out a theory of SCL currents in defect insulators. If the insulator contains traps, a large fraction of the injected space charge will condense therein which means that the free carrier density will be much lower than in a perfect insulator, such that

$$J \alpha \frac{\theta V^2}{t^3} \quad \ldots.(18)$$

Where θ is ratio of free to trapped charge. Clearly smaller

the value of θ, more effective will be the traps in immobilising the injected carriers. Therefore a higher injection level or applied bias is required for the current flow. The occupancy of traps is a function of temperature and so the SCL current show temperature dependence. Lampert [53] has pointed out that if sufficient charges are injected into the insulator, the traps will become filled. Any additional injected charge can then exist as free charges in the conduction band contributing totally to the current. Beyond trap filled limit (TFL) the I-V characteristics is given by Mott-Gurney law [Equation (15)].Lampert [54] reports that for double injection of carriers at very high voltages, $J \alpha V^3$ with both recombination and space charge playing a role in limiting the current. Pulfrey and Shousha [55], Geppert [18] derived expressions for computing the effects of the space charge on the current density of electrons tunneling. Accordingly, space charge is shown to severely limit the tunnel current if large traps are present in the insulator. Lamperts [53] analysis of a simple model for electron space charge limited current in a trap free insulator has revealed existence of negative resistance effects and oscillations in Current-Voltage characteristics.

1.5 Forming Process , breakdown and voltage controlled negative resistance (VCNR)

With the application of the increasing voltage, it is found that at a certain voltage (V_f), the metal-insulator-metal (MIM) devices undergo a radical and permanent change in their electrical properties and the current increases by 3-4 orders of magnitude. This process is called forming and V_f is known as the forming potential [15]. V_F is found to be independent of the thickness of

the dielectric. Forming process is a distinct and novel high field phenomenon, different from dielectric breakdown discussed later.`Forming' process is distinguished from dielectric breakdown (which destroys the insulator) in terms of establishment of a negative resistance region in the current-voltage characteristics by a non-destructive breakdown of the dielectric/insulator. It depends on the fabrication method, electrodes, impurity content, prevailing atmosphere, ambient temperature and pressure [56-59]. The studies on SiO_x [60], Al_2O_3 [57], GeO_2 [61], V_2O_3 [62], AlN [63] having sandwiched structures have shown forming with respective characteristic potentials. The formed MIM devices normally show voltage controlled negative resistance and even switching and memory phenomena [15]. The mechanisms which give rise to VCNR are processes : (i) in which the Joule heating of the conduction electrons causes a change in their number or in their mobility (ii) in which special semi-permanent space-charge distributions are set up, and (iii) which involve a phase change or atomic rearrangement in the insulator [15].Various models put forward to explain forming and VNCR [60,64-67,15] are summarised in Table 1.2 and Table 1.3, respectively. So far, anodically prepared and r.f. sputtered Al_2O_3 MIM structure have been reported to exhibit forming and VCNR [56,58,68-70], with post VCNR region noisy and unstable. Dielectric breakdown occurs both in `formed' and unformed systems. It is characterized by a sudden change in current by a few orders of magnitude at a given voltage and is accompanied by total disappearance of the insulating properties. In unformed samples, breakdown is accomplished directly whereas in formed sample it usually occurs beyond the VCNR region. Dielectric strength of an insulator is defined as the

maximum voltage gradient which it can withstand before failure/destruction occurs. MIM devices suffer breakdown of mainly two types a) single hole and/ or b) maximum d.c. voltage [71-72]. Single hole breakdown arises when conducting channels are created at flaws in the dielectric at high electric fields, resulting in heavy current. Maximum d.c. voltage (V_{br}) breakdown occurs due to thermal effects produced by enhanced current via flaws or defects. According to Gould and Hogarth [73] dielectric breakdown in an unformed device normally occurs at much higher potential than V_{br}. Various other breakdown processes observed in dielectrics are termed as thermal [71], avalanche [74-75] and intrinsic [76]. In thermal breakdown the heat generated by the ionic current is faster than the device can dissipate. Since the thermal conductivity of the insulator is very low, a channel of molten material or jagged hole is obtained. Sometimes a `dendrite' structure is formed due to discharge of metal ions, bridging the gap between electrodes. Breakdown strength is inversely proportional to thickness of insulator. In avalanche process [77], dielectric breakdown begins with the appearance of a number of electrons in the conduction band. These electrons are accelerated rapidly by the high field in the dielectric, and attain high kinetic energies. Some of the kinetic energy is transferred, by collisions, to valence electrons,which are there- by elevated to the conduction band. Intially some electrons initiate this process, it multiplies itself, and an avalanche of electrons is obtained in the conduction band. The current through the dielectric increases rapidly, and the dielectric is apt to locally melt, burn or vapourize. The breakdown strength increases with the decrease of insulator thickness. Intrinsic breakdown [76] occurs when the energy gained by the

conduction electrons from the field is transfered to the bulk structure and phonon emission takes place. The rate of gain and loss of energy by the conduction electrons above a certain critical field E_c, results in energy imbalance leading to breakdkown. It occurs at room or low temperatures and is dependent on thickness of the insulator. Shousha, Pulfrey and Young [78] proposed a model for breakdown in thin dielectrics. Accordingly, non-destructive electron avalanche precedes the thermal runaway process. Furthermore, breakdown occurs in a narrow channel of the insulator. This may take place even at fields lower than the normally accepted dielectric strength provided the initial temperature rise caused by the avalanche is sufficiently high. Most theoretical work on breakdown has been concerned with mechanism associated with impact ionisation, the condition for electron runaway and breakdown fields. Ridley [79] suggested a breakdown on the assumption of presence of large irregularities at electrode interfaces. Greatly enhanced current injections at such irregularities produces high temperature filaments in which dissociation of ion pairs takes place. The resulting positive ions drift to the cathode, producing a positive feedback effect on the current leading to instability and current runaway. Budenstein [80] proposed that the breakdown mechanism involves the creation of gaseous channel through the dielectric. The formation of gaseous channel is ascribed to energy supply from the external source and its storage in solid by polarisation, collision ionisation, trapping and atomic displacement resulting in a change in the local charge balance and in broken molecular bonds. Jonscher and Lacoste [83] proposed a breakdown mechanism connected with the existence of point defects, in the insulator. On the application of a high field,

charge carriers are assumed to generate additional defects leading to the formation of defect clusters . These clusters in turn can grow by further defect generation into a highly conducting channel connecting the electrodes and producing destructive breakdown. The results of anodically grown Al_2O_3 were found to agree well with predictions of avalanche breakdown model [82]. However de wit et al. [83] found that breakdown in anodically prepared Al_2O_3 films is better explained by filamentary approach reported by Ridley [79].

Present work

In the present thesis ,efforts have been made to investigate the electronic conduction mechanisms in Al-Al_2O_3-Al sandwiches and understand the phenomena in detail. Al_2O_3 has been chosen as the insulator because it is stable and can be prepared by thermal oxidation in a relatively easy manner. Some of the known parameters of aluminium and Al_2O_3 are summarized in Table 1.1 . The various conduction mechanisms have been analysed and barrier height values determined for different thicknesses of the insulator.The 'Forming' process followed by voltage controlled negative resistance and dielectric breakdown of Al_2O_3 have been examined in detail in the light of existing reports in the literature.

TABLE 1.1 : Some known parameters of Al and Al_2O_3

Parameters	Al	Al_2O_3
Work-function	4.2 eV	5.4 eV
Band-gap energy	—	7 eV
Dielectric-constant(K) high frequency ($K = n^2$)	—	3.07, 4.5
low frequency	—	8.5
Density ($g\ cm^{-3}$)	2.7	3.0 - 3.97
Refractive index (n)	—	1.76
Atomic or Molecular wgt.	26.98	101.96
Phase	Crystalline f.c.c.	Amorphous or Crystalline (several phases)

TABLE 1.2 : MODELS PREPARED FOR THE FORMING PROCESS AS SUMMARIZED BY DEARNALEY et al. [15]

Reference	Model Description	Dependence on Electrode	Dependence on Insulator	Dependence on Atmosphere
Hickmott [66]	Schottky ionisation of impurities near middle of band gap : formation of localized states for impurity band band and space charge to aid injection of electrons.	Uncertain	V = ½(Energy gap) and Voltage dependent	Uncertain
Simmons and Verderber [62]	Injection of ions from anode to form broad impurity band with a sharp top band bending from space charge	Impurity levels depend on species & band bending on work fn.	V < ½(Energy gap) and Voltage dependent	Independent
Dearnaley [67]	Propagation of conducting filament through insulating film.	Forming initiated at anode	V related to breakdown strength or crystal formation energy.	Oxygen prevents filament propagation or initiation
Barriac et al. [68]	Local fusion of insulator or electrode with subsequent ion injection. Also traps are formed.	not discussed	not discussed	Oxygen neutralises the ions which constitute the space charge
Greene et al. [69]	High field eletrolysis with injection of vacancies from cathode.	Dependent on anode	V = Gibbs free energy of formation of insulator	Oxygen may cause competing reactions at anode

TABLE 1.3 : MODELS PROPOSED FOR THE OBSERVATION OF VOLTAGE CONTROLLED NEGATIVE RESISTANCE (VCNR) AS SUMMARIZED BY DEARNALEY et al. [15]

Reference	Mechanism of VCNR	Dependence on V(volts)	Temperature Dependence
Hickmott [66]	Some process dependent on a high field which reduces the number of impurity centres which contribute to conduction	Fixed by relative positions of impurity levels. Observes relation to bulk properties	Trapping is temperature dependent
Simmons and Verderber [62]	Top of impurity band in the centre of insulator falls below the anode ferai level. Hence charge trapped in depletion layer near anode and reduction in current since only electrons below the top of impurity band contribute	V depends on electrode and impurity states should have sharp maximum energy	Trapping of space charge is temperature dependent
Barriac et al. [68]	Injection of electrons immobilizes ions by trapping	V dependent on temperature	Trapping of electrons by ions is temperature dependent
Dearnaley [67]	Rupture of conducting filament by joule heating	Depends on distribution of filament resistance hence on insulator and not on electrodes.	generation of filament involves dielectric relaxation and ionic motion

CHAPTER 2

EXPERIMENTAL DETAILS AND PROCEDURES

In this chapter, we discuss the procedures adopted for cleaning the glass substrates, preparation of metal-insulator-metal sandwiched structures, estimation of oxide thickness through capacitance measurements and obtaining I-V characteristics of the Al-Al_2O_3-Al junctions.

2.1 SUBSTRATE CLEANING

A thoroughly cleaned substrate is a prerequisite for the preparation of films with reproducible properties. The choice of cleaning procedure depends on the nature of the substrate, the type of the contaminants and the degree of cleanliness required. Residues from manufacturing and packaging, lint, fingerprints, oil and airborne particulate matter are examples of frequently encountered contaminants. The microscope glass slides and photographic plates (after the removal of emulsion) were used as substrates after cleaning in the following manner [12,85]:
Glass slides were first cleaned with a soap detergent and then dipped in a solution of chromic acid (10 ml aqueous $Na_2Cr_2O_7$ in 200 ml H_2SO_4) at 50°C. Subsequently,they were washed in vapours of trichloroethylene, acetone, methanol and distilled water in succession. Drying of these glass slides was done afterwards with a Philips infra-red lamp. Glass slides thus cleaned were stored in a dust free chamber. Just prior to use, the slides were wiped with lint free tissue paper.

.2 PREPARATION OF Al-Al_2O_3-Al SANDWICHED STRUCTURE

Firstly, thin films of aluminium (99.999% purity) were deposited onto the cleaned glass slides. For this purpose a mask as shown in figure 2.1a was used. This allowed the aluminium films deposition to be in the form of strips 1mm wide. The mass-thickness (t) of the evaporated film was monitored by the amount of aluminium using the relation $M = 2\pi R^2 \rho t$, where M (g) is the mass in grams taken for evaporation, ρ(g cm^{-3}) is the density of the material and R (cm)is the distance between the source of evaporation and the substrate for thickness t(cms). The films deposited were 500nm thick. For evaporation, tungsten filaments cleaned by resistive heating at 10^{-5} torr were used . For weighing the appropriate amount of aluminium, a balance having sensitivity of 0.1 mg was employed. The deposition was carried out in a vacuum coating unit constructed in the laboratory based on Hindhivac pumping system model 4D65. After attaining the working pressure of about 10^{-5} torr, a low voltage high amperage current was passed through the filament for about 15 seconds for evaporation of aluminium from the tungsten filament source. The vapours were collected onto the masked glass slide. Thermal oxidation of the aluminium layer upto a certain thickness was subsequently achieved by introducing it in an electric furnace (equipped with a temperature controller Indotherm model 401 having accuracy of ±1°C) at temperatures 50°C, 100°C, or 150°C for a duration of 24 hours [20,84] in air or oxygen atmosphere. After the formation of oxide layer the glass slides were returned to the evaporator. The upper aluminium electrode 1mm wide and 200nm thick was then deposited using a mask (figure 2.1b) such that a cross-stripped structure is formed (figure 2.2a).The thickness of this electrode

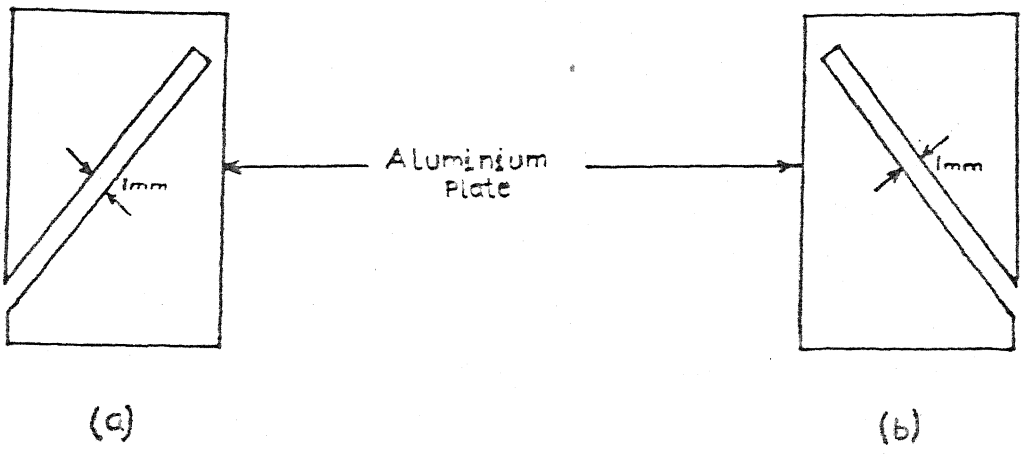

Fig 2.1 a,b Masks used for deposition of aluminium films

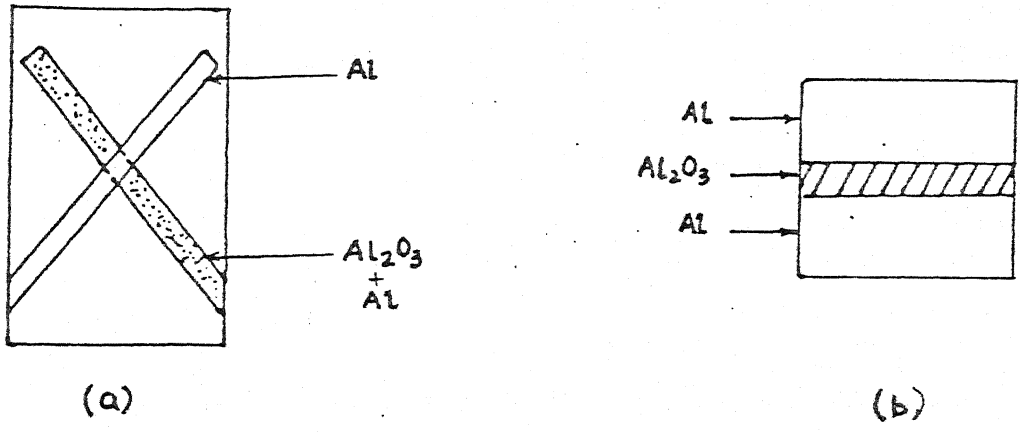

Fig 2.2 (a) Cross strip structure and
(b) Cross-sectional view of Al-Al_2O_3-Al

is intentionally kept high as for lower thickness the current is strongly influenced by humidity [86].

2.3 ESTIMATION OF OXIDE THICKNESS

The oxide thickness (t cms) can in general be determined by measuring the charge storage capacity of the Al-Al_2O_3-Al structure at low frequencies, taking a dielectric constant of K = 8.5 [58,87-88] for Al_2O_3 and using the relation

$$\frac{A}{C_m} = \frac{t}{\epsilon_o K} \quad \ldots (19)$$

where ϵ is permittivity of free space (8.85×10^{-14} F/cm) and A(cm^2) is the geometrical area of the junction. This method holds good for bulk samples. However, in case of thin film junctions, this can lead to serious error in estimating the dielectric thickness as the measured capacitance now includes a substantial contribution from the interface [89-92].According to Hebard et al [92] measured capacitance (C_m) can be considered as series combination of the interfacial (C_i) and geometrical components such that

$$\frac{A}{C_m} = \frac{A}{C_i} + \frac{t}{K\epsilon_o} \quad \ldots (20)$$

The interfacial contribution has been determined [93] by extrapolating the plot of A/C_m versus Oxide thickness (t), measured by optical interferometry,for Al-Al_2O_3-Al structures as $C_i/A = 1.62\ \mu f/cm^2$. C_m is measured at 100 Hz.

In the present case, thickness of the aluminium oxide is estimated by measuring the capacitance of Al-Al_2O_3-Al structures using a Keithley 4192A LCR impedance bridge at a test voltage of

20 mV at 100 Hz and taking the value of C_i/A given above for this system.

2.4 CURRENT-VOLTAGE CHARACTERISTICS

Thin copper wires were attached with silver conducting paint at the ends of the cross strips for applying the voltage (V_1 and V_2) and measuring the currents (I_1 and I_2). The electrical circuit used for obtaining the current-voltage characteristics is shown in figure 2.3a. The current through the junction was measured with a Keithley 611 electrometer and the voltage across it was monitored by a Keithley 610 nanovoltmeter. The power supply employed was knick-precision current/voltage source equipped with a voltage control knob. Also a 5KΩ potentiometer was put in series with the power source for the stability of the current through the circuit and for allowing further control of voltage across the junction. At each voltage value, sufficient time (say 1-2 minutes) was given to obtain steady state and only after that current value was recorded.

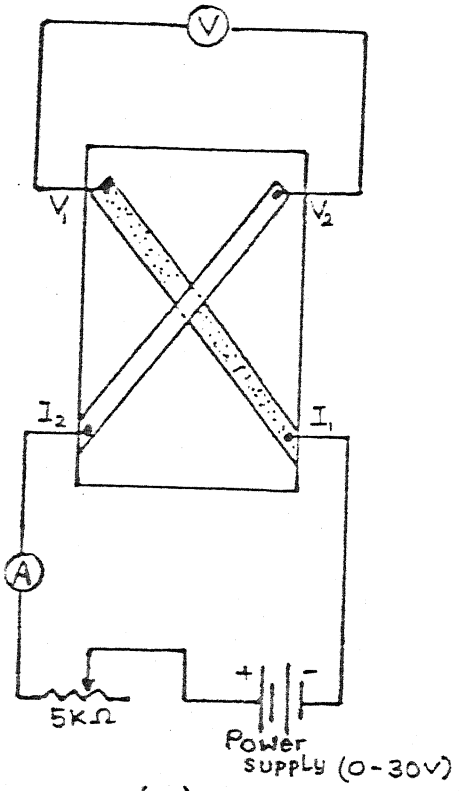

(a)

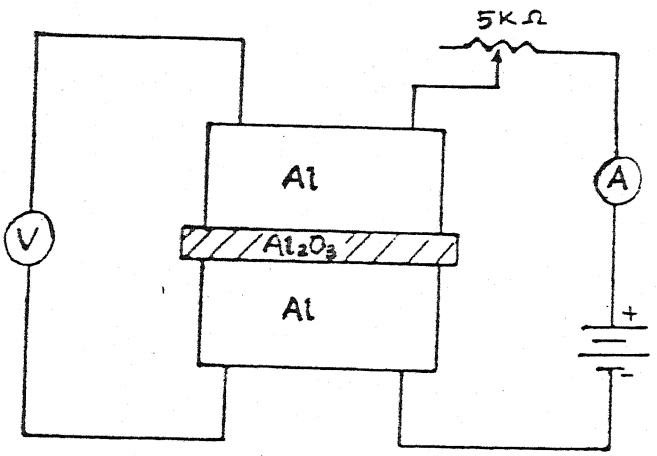

(b)

Fig 2.3 Circuit used for Current-Voltage characteristics of Al-Al_2O_3-Al structures with (a) cross strip arrangement (b) a cross-sectional view

CHAPTER 3

RESULTS AND DISCUSSION

3.1 Formation of Oxide layers:

Aluminium is not stable and reacts spontaneously with oxygen when exposed to air or oxygen even under ambient conditions to form the thermodynamically favoured oxide [84,93]. The driving force for the reaction is the Gibbs energy change associated with the formation of oxide from the reactants. Moreover, once the oxide layer has developed on the surface, further reaction occurs only if one (or both) of these species is able to penetrate the barrier,formed by the oxide at either the oxide-metal or oxide-oxygen interface. Hence, the rate of oxidation does not depend on the thermodynamics of the reaction but on the kinetics of the system. The rate determining step may be one of several stages including transport of metal or oxygen atoms through the oxide, mass or electron transport across one of the interfaces or electron-transport process associated with chemisorption [93]. Aluminium oxide is reasonably stoichiometric having chemical composition Al_2O_3 with low defect concentrations, and can give effective protection to aluminium in environments of high oxygen activity. As an oxide layer grows, the system may be subjected to stresses causing crack or spall of oxide which, in turn, exposes the metal directly to the environment and increased oxidation occurs. The stresses may be internal, generated by the oxide growth process itself; thermal,arising due to differential thermal expansion or contraction effects between the oxide layer and metal, and external, caused by the applied load etc. Generally specific volume of the oxide is not the same as that of the metal from which

it is formed. Pilling-Bedworth ratio (Ø) is defined as

$$Ø = \frac{\text{molecular volume of oxide}}{\text{atomic volume of metal}} = \frac{M_o d_m}{n^*_m (M_m) d_o}$$

Where M_m is the atomic weight of the metal atom, M_o the molecular weight of the oxide, n^*_m the number of metal atoms per molecule of oxide and d_m and d_o are the densities of metal and oxide, respectively. This ratio Ø distinguishes oxide layers with regard to their protective abilities. If Ø is smaller than unity (eg. Hg,Ba etc) the oxide layer fails to cover the entire metal surface and forms discontinuous or non-protective coating through which oxygen can readily pass. Thus the rate of reaction is not reduced by growth of the oxide layer.The mass of oxide formed per unit surface area at con tant temperature is directly proportional to the time of heating. On the other hand, if Ø is greater than unity, the oxide occupies larger volume than the metal and so the oxide will, in this case, be protective.For oxidation of aluminium, the value of Ø lies between 1.287 and 1.7 depending upon the type of Al_2O_3. Consequently, the oxidation of aluminium proceeds slowly and stops eventually. Pilling-Bedworth ratio (Ø) also gives estimate of the magnitude and nature of stresses generated during oxidation.Since Ø is greater than unity, oxide layer is subjected to lateral compression. Three factors generally considered are :(i) magnitude of the lateral stresses due to compressions within the oxide layer, (ii) the cohesion of oxide particles and (iii) adhesion of the layer to the metal surface. With the volume ratio (Ø) slightly above unity one would not expect much trouble from stresses in the surface layer. However , with greater volume ratio, mechanical deformation of layers may result, e.g. blistering occurs where adhesion is weak and cohesion is strong and shear - cracking

where adhesion is strong and cohesion is weak. The effect of lateral compressive stress is not significant as Ø (1.287-1.7) is slightly above unity. Sometimes blistering results though, indicating that adhesion is weak and cohesion is strong. Aluminium oxide layer formed by thermal oxidation is amorphous in nature and quite stable upto about 500°C and transforms to crystalline γ - Al_2O_3 above this temperature as revealed by electron diffraction studies. The temperatures used for the oxidation in the present work were 50 , 100 , and 150°C, which are well below the transition temperature to ensure stable amorphous Al_2O_3 films. The thickness of Al_2O_3 depends upon factors such as temperature, time and humidity. The time for oxidation in each case was kept constant (i.e. 24 hours) and humidity in room remained practically the same during the oxidation cycle. The thickness of the oxide layer is therefore expected to vary mainly due to increase in the temperature . The thickness in each case was estimated by measuring the capacitance of the samples using the impedance bridge HP 4192 at 100 Hz.The details of the measurement are given in section 2.3. Table 3.1 lists the capacitance values for various oxidation conditions. The measured capacitance is a series combination of two components, interfacial & bulk. Only the bulk part of the capacitance depends on the oxide thickness. Therefore the interfacial contribution was to be separated from the measured values of capacitance for the estimation of oxide thickness. According to Hebard et al [92] interfacial capacitance is 1.62 $\mu F/cm^2$ for Al-Al_2O_3-Al system with oxide thickness (< 36nm)and is independent of applied voltage. The thickness of oxide layers determined using Equation (20) are given in Table 3.1 alongwith thickness values estimated by neglecting interfacial effects. It

TABLE 3.1 : Estimated values of oxide thickness from the measured capacitance (C_m) for Al - Al_2O_3 - Al system having junction area (A) of 10^{-2} cm^2 and taking dielectric constant (K) 8.5 and permittivity of free space(ϵ_o) 8.85 10^{-14} F/cm

Sample	Temperature of oxide formation °C	Measured capacitance per unit area (μ F/cm^2)	Thickness t(nm)	
			t_1	t_2
1	50	0.888	3.8	8.5
2	100	0.829	4.4	9.1
3	100	0.790	4.9	9.5
4	150	0.725	5.7	10.4

t_1 - taking interfacial capacitance per unit area (C_i/A) 1.62 μF/cm

t_2 - taking total measured capacitance due to bulk of Al_2O_3 itself i.e. assuming no contribution from interfacial effects

is clear from this data that thickness of oxide layer increases with the oxidation temperature. Though oxidation can occur even at room temperature, it is allowed to take place at 50°, 100° and 150°C in the present study for sake of ensuring uniformity and stress release in the growing oxide films. Initial experiments using larger junction areas failed to provide acceptable Al-Al_2O_3-Al sandwiches presumably due to the presence of pinholes in oxide films ,junction shorting etc. Therefore various junction areas were tried out and finally 0.1 cm x 0.1 cm size was adopted for the study.

3.2 Current-Voltage characteristics of Al-Al_2O_3-Al Junction

The general behaviour of various Al-Al_2O_3-Al junctions is that the current-voltage characteristics exhibit non-linearity, as depicted schematically in Fig.3.1. The curve can be divided into three distinct categories showing (a) marginal increase in current, (b) sharp increase in current by a few orders of magnitude, and (c) anamalous behaviour in the form of a negative resistance followed by fluctuations (or noise) in the current with respect to the applied voltage. Fig 3.2 (a-d) shows the I-V characteristics of four Al-Al_2O_3-Al junctions in region (a) only. Since the thickness of Al_2O_3 layer is less than 10 nm in all the cases, applied bias of even a few volts across the junction induces electric field of the order of 10^6 V/cm. At such a high field there are five principal d.c. electronic conduction modes [45]: (a)Ohmic, (b)Space charge limited, (c)Tunneling, (d)Schottky emission, and (e)Poole-Frenkel effect.A single conduction process may not always be responsible for the entire I-V characteristics. However, analysing the experimental data carefully, it is possible to indentify the range

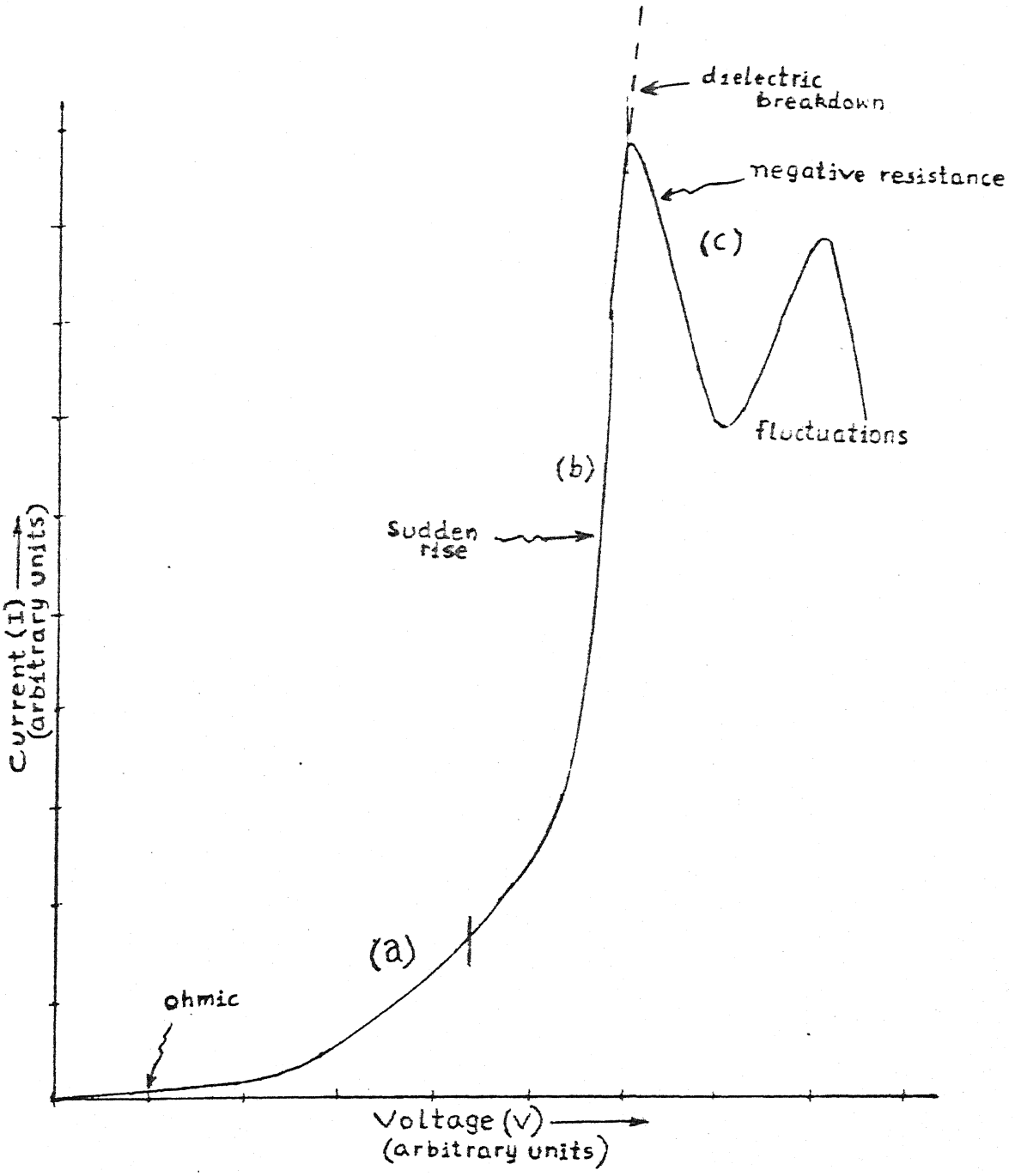

Fig.3.1 Schematic diagram of current(I) - Voltage(V) characteristics of Al-Al_2O_3-Al structure showing three distinct categories (a), (b), (c)

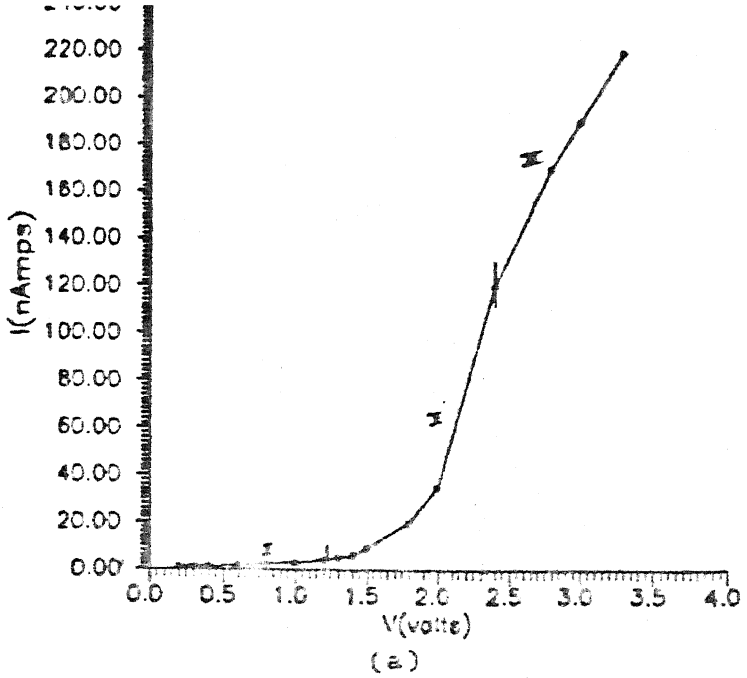

(a)

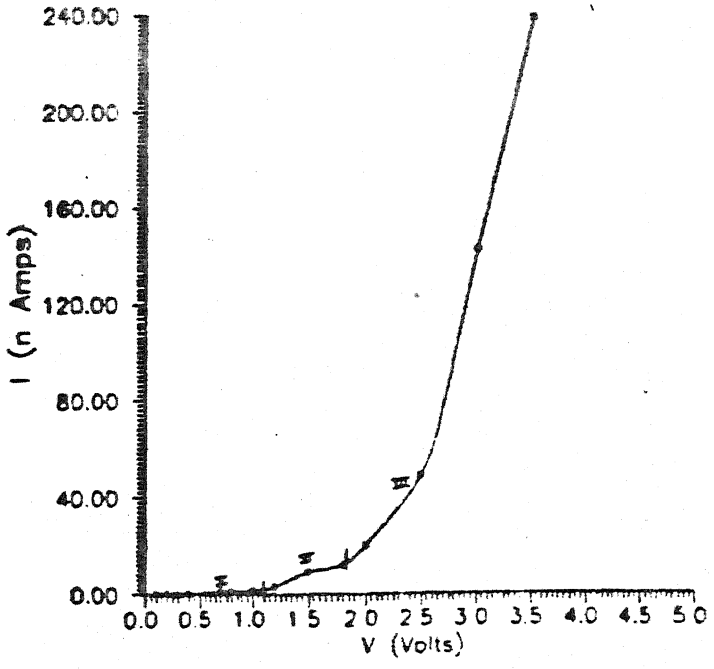

(b)

Fig.3.2 I - V characteristics of the Al-Al_2O_3-Al structure for insulator thickness (a) 3.8 nm (b) 4.4 nm (c) 4.9 nm (d) 5.7 nm

continued . . .

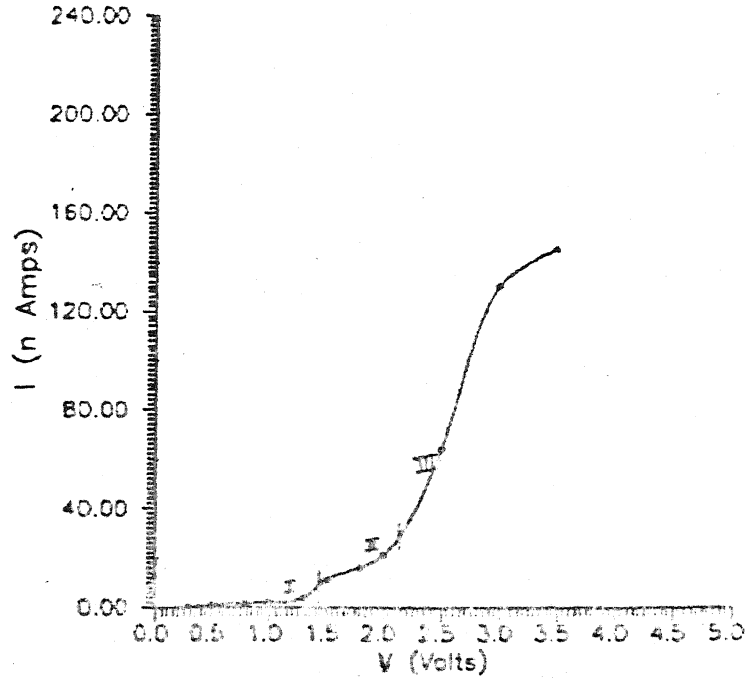
240.00
200.00
160.00
120.00
80.00
40.00
0.00
I (n Amps)
0.0 0.5 1.0 1.5 2.0 2.5 3.0 3.5 4.0 4.5 5.0
V (Volts)
I
II
III

(c)

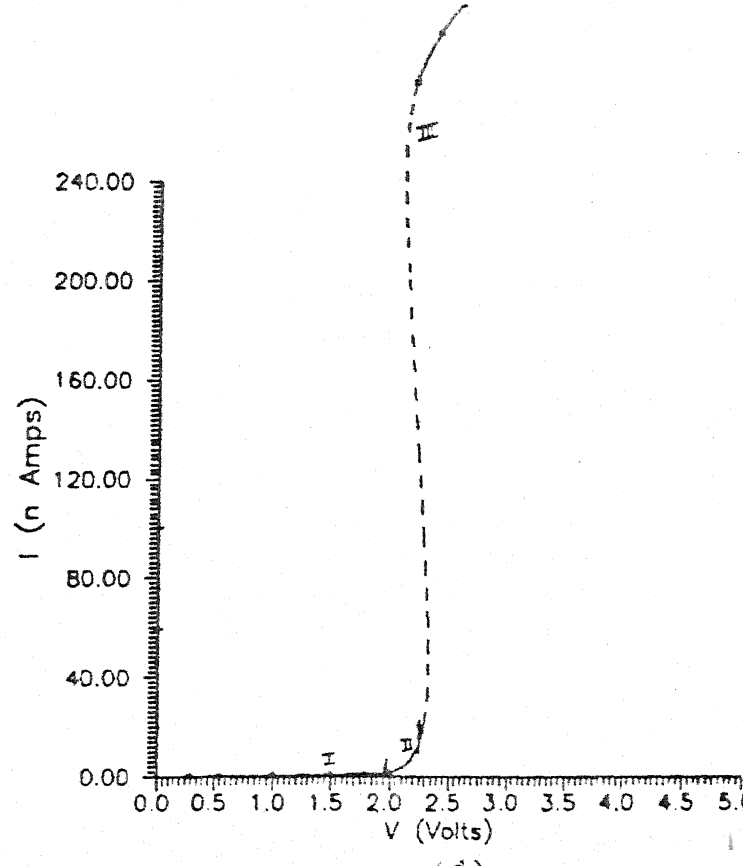
240.00
200.00
160.00
120.00
80.00
40.00
0.00
I (n Amps)
0.0 0.5 1.0 1.5 2.0 2.5 3.0 3.5 4.0 4.5 5.0
V (Volts)
I
II
III

(d)

linearity in current involves voltages starting from a certain value and upto about 3 volts . The plots in early regions marked (I) show linearity indicating ohmic behaviour of junctions.One way to understand the underlying conduction process is to examine the power dependence of voltage on current [27] i.e. $I = AV^n$, where exponent n stand for the power dependence and A represents the proportionality constant involving insulator thickness. Taking logarithms one gets

$$\log I = \log A + n \log V$$

Thus log I versus log V plot should be a straight line with a slope giving the power dependence, However, if n takes a different value in certain voltage range, another straight line should appear with a new slope. The transition from one power dependence to another may be sharp or gradual with respect to the voltage. This means that it either occurs at a given potential or spreads over a voltage range. Fig. 3.3 (a-d) depicts log I versus log V plot obtained from the data in Fig.3.2 (a-d). These plots show straight lines or non-linearity in various regions. The slopes of straight lines in same regions of different samples are given in Table 3.2. It is advisable however to examine these results in conjunction with other plots viz.ln I versus $V^{½}$ shown in Fig. 3.4 (a-d). The various regions have been marked clearly as (I), (II), (III) . Since such a plot is more sensitive to changes in the slope, regions are first marked here and ranges noted for illustrating the corresponding regions on I-V and logI-logV plots given in Fig.3.2 (a-d) and Fig. 3.3 (a-d), respectively. The voltage range of various regions are summarized in Table 3.3. Note that, except for the thinnest oxide layer sample (3.8 nm) the voltage at which

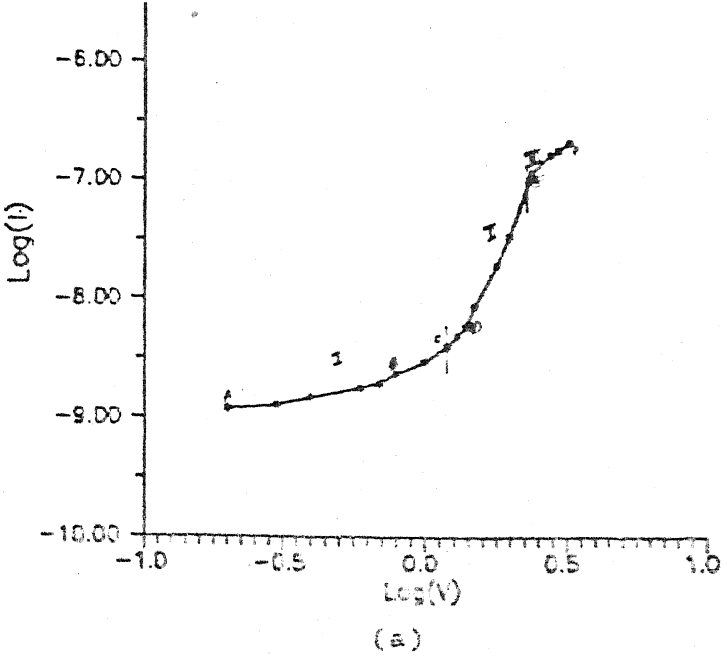

(a)

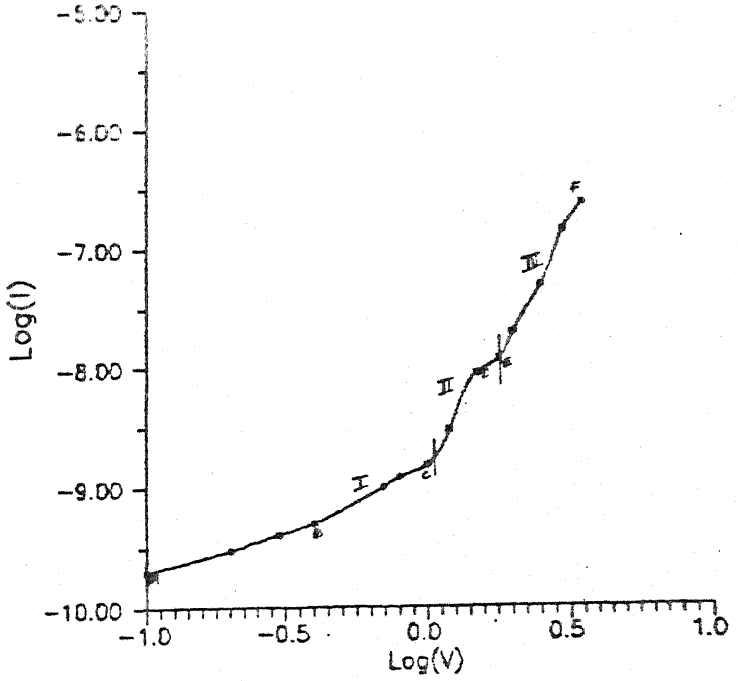

(b)

Fig.3.3 Log I - Log V characteristics of the Al-Al_2O_3-Al structu for insulator thickness (a) 3.8 nm (b) 4.4 nm (c) 4.9 nm (d) 5.7 nm

continued . . .

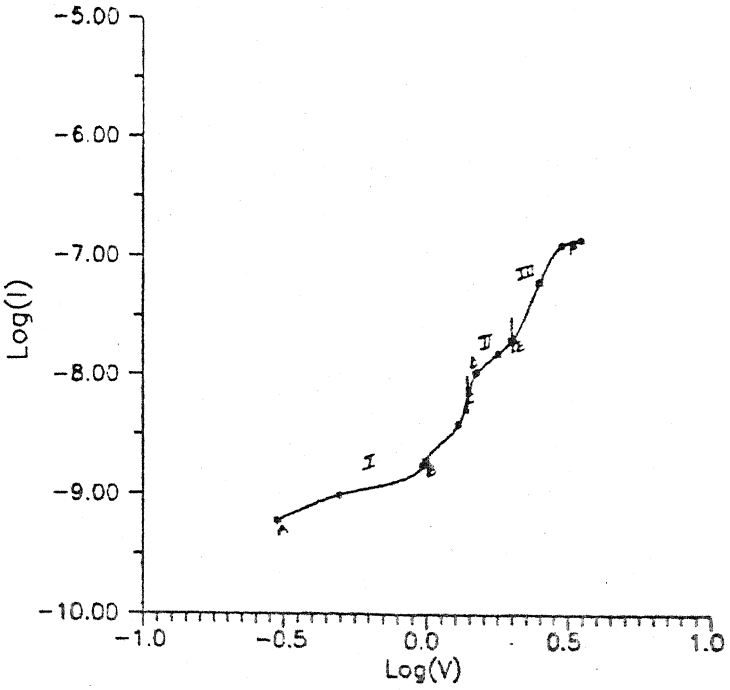
-5.00
-6.00
-7.00
-8.00
-9.00
-10.00
Log(I)
-1.0
-0.5
0.0
0.5
1.0
Log(V)
I
II
III

(c)

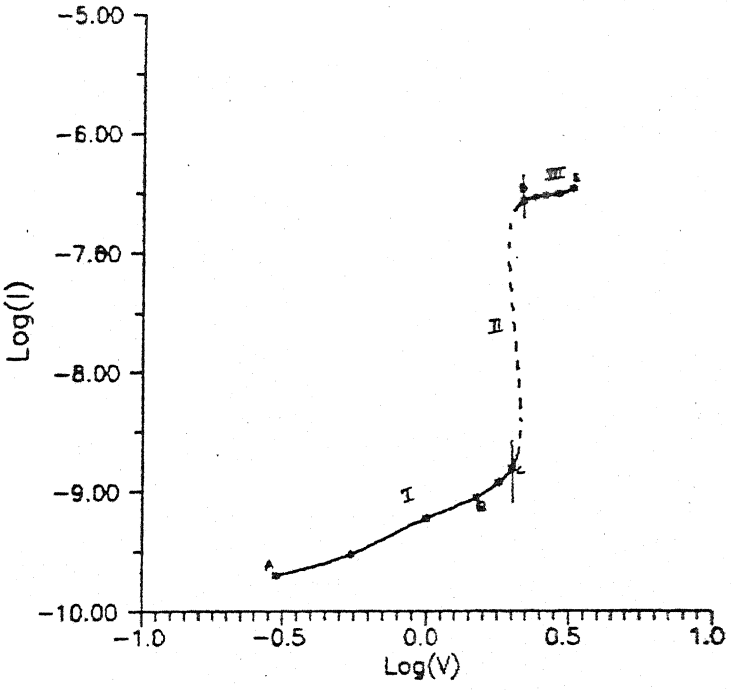
-5.00
-6.00
-7.00
-8.00
-9.00
-10.00
Log(I)
-1.0
-0.5
0.0
0.5
1.0
Log(V)
I
II
III

(d)

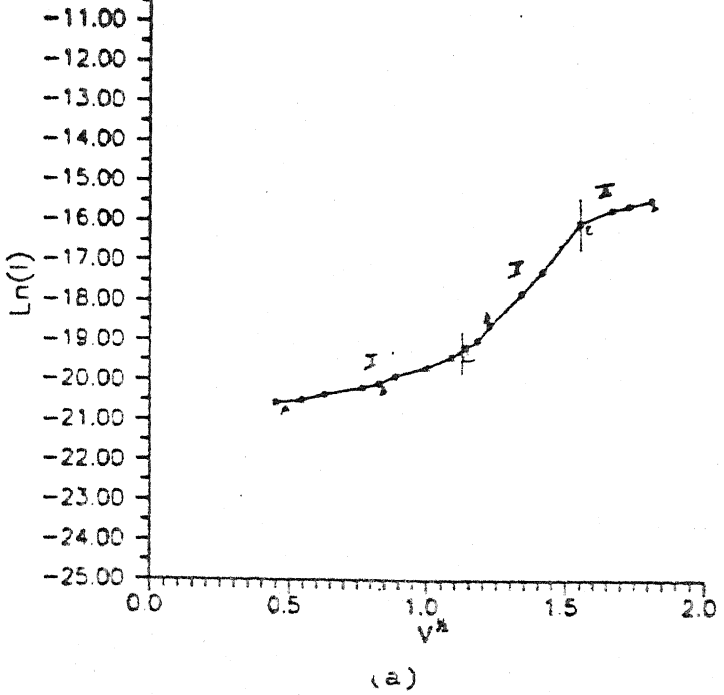

(a)

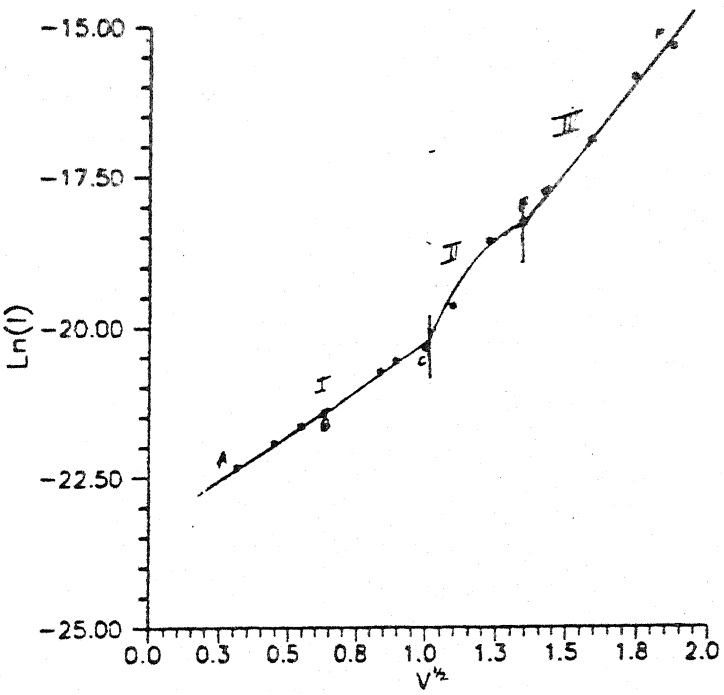

(b)

Fig.3.4 Ln I - $V^{1/2}$ characteristics for Al-Al_2O_3-Al structure for insulator thickness (a) 3.8 nm (b) 4.4 nm (c) 4.9 nm (d) 5.7 nm

continued . . .

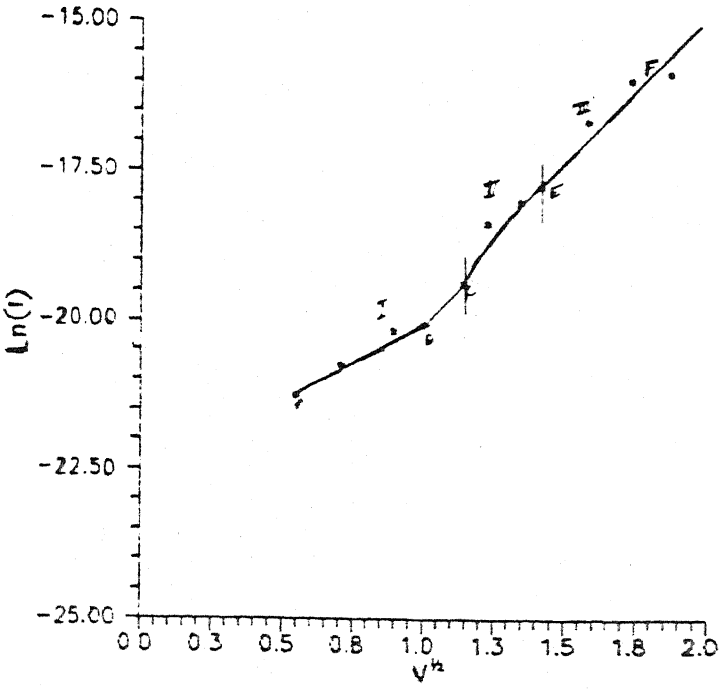
-15.00
-17.50
-20.00
-22.50
-25.00
Ln(I)
0.0
0.3
0.5
0.8
1.0
1.3
1.5
1.8
2.0
V^½
I
II
E
F

(c)

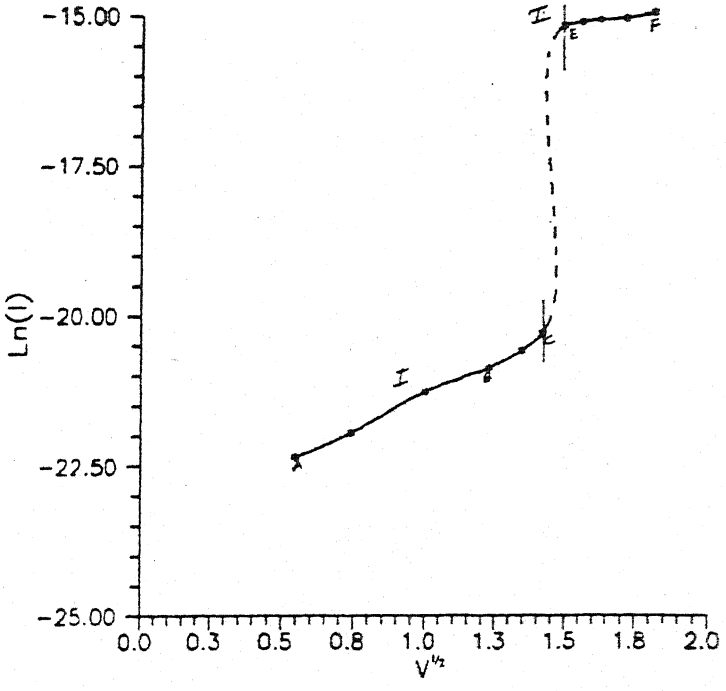
-15.00
-17.50
-20.00
-22.50
-25.00
Ln(I)
0.0
0.3
0.5
0.8
1.0
1.3
1.5
1.8
2.0
V^½
I
II
E
F

(d)

TABLE 3.2 : Slopes of straight lines in different regions of $\log I$-$\log V$ plot of Al-Al_2O_3-Al juntion

Al_2O_3 film thickness (nm)	I	II	III
3.8	0.42 1.36	5.33	2.52
4.4	0.69 1.17	—	4.66
4.9	1.06 3.92	—	4.48
5.7	0.95 2.03	—	0.52

TABLE 3.3 : Voltage ranges corresponding to regions I , II and III , (Fig. 3.2) of the I - V characteristics of Al-Al_2O_3-Al junctions

Thickness (nm)		I	II	III
t_1	t_2	Voltage range(V)	Voltage range(V)	Voltage range(V)
3.8	8.5	$\leq$ 1.23	1.23-2.4	$\geq$ 2.4
4.4	9.1	$\leq$ 1.08	1.08-1.82	$\geq$ 1.82
4.9	9.5	$\leq$ 1.44	1.44-2.1	$\geq$ 2.1
5.7	10.4	$\leq$ 1.98	1.98-2.25	$\geq$ 2.25

t_1 - taking interfacial capacitance per unit area (C_i/A) 1.62 $\mu F/cm^2$

t_2 - taking total measured capacitance due to bulk of Al_2O_3 itself i.e. assuming no contribution from interfacial effects

transition occurs from region I to II and from II to III increases with the Al_2O_3 thickness. Fig. 3.5 (a-d) and Fig.3.6 (a-d) show log(I/V) versus $V^{\frac{1}{2}}$ and $\log(1/V^2)$ versus 1/V plots , respectively. The plots in Figures 3.2 to 3.6 have been examined in detail to determine the conduction mechanisms in the various regions . The characteristics of various conduction mechanisms as reported in literature are summarized in Table 3.4. These results suggest that the I-V characteristics of thin Al_2O_3 films cannot be explained on the basis of a particular mechanism [20,34,39]. These samples exhibit ohmic behaviour at low voltages and perhaps schottky emission and/or Poole-Frenkel effect become important when the voltage is increased. This is indicated by the linearity in the lnI - $V^{\frac{1}{2}}$ plots [35,41,45,46]. Analysis of these plots using equations (10)&(11), yields reduced values for the barrier height as compared to the theoretically estimated values (Table 3.5), possibly due to the interaction of image force with the applied field [41]. The barrier height increases with increase in the oxide thickness. This observation is in agreement with the results of Vodenicharov and Christov [41] and indicates the presence of Schottky mechanism. A log (I/V) - $V^{\frac{1}{2}}$ plot for different samples is found to be non-linear indicating the absence of Poole-Frenkel effect in region II [45,46]. Instead, a horizontal line is invariably found, implying thereby ohmic behaviour of the junction [45]. The slopes of straight lines in the ln I - $V^{\frac{1}{2}}$ plots are used to determine the conduction coefficient (β_s) for Schottky emission. Table (3.5) lists the values of β_s along with the corresponding values estimated theoretically [35] from the relation, $\beta_s = (e^3/4\pi \epsilon_o K^* t)^{\frac{1}{2}}$. Here K^* is the high frequency dielectric constant, and the other symbols have their usual

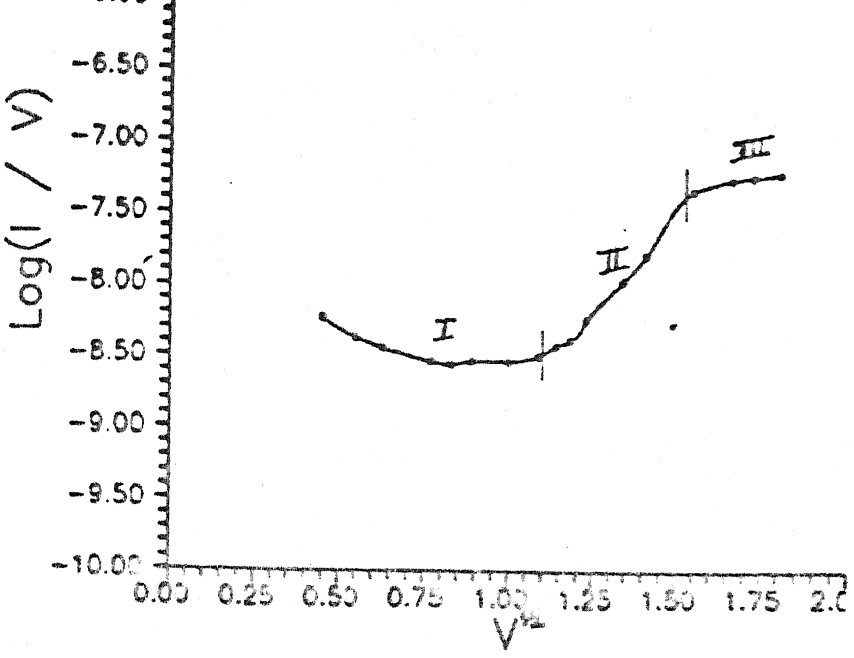

(a)

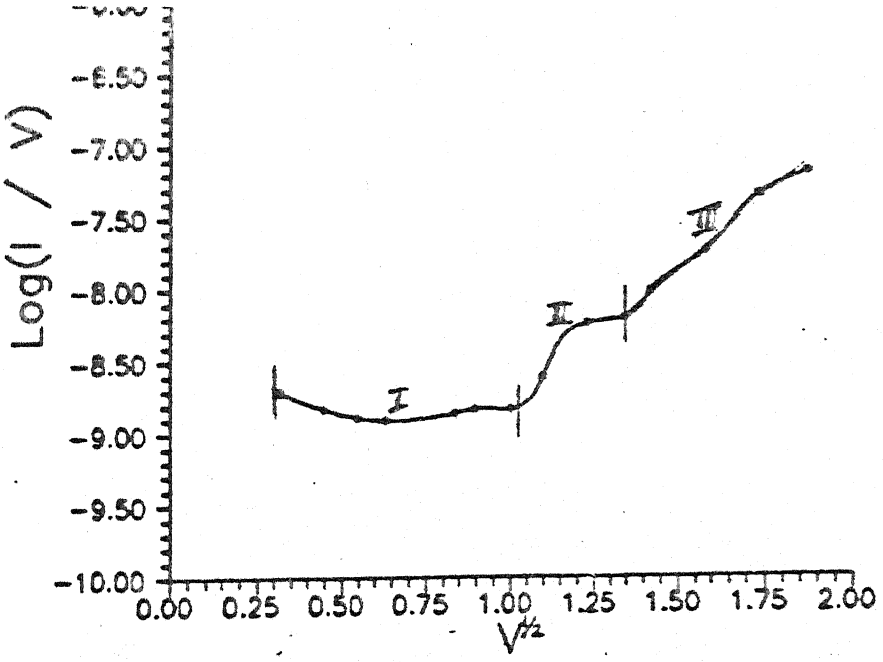

(b)

Fig 3.5 $Log(I/V)-V^{1/2}$ plots of Al-Al_2O_3-Al structures for insulator thickness (a) 3.8nm (b) 4.4nm (c) 4.9nm (d) 5.7nm

continued . . .

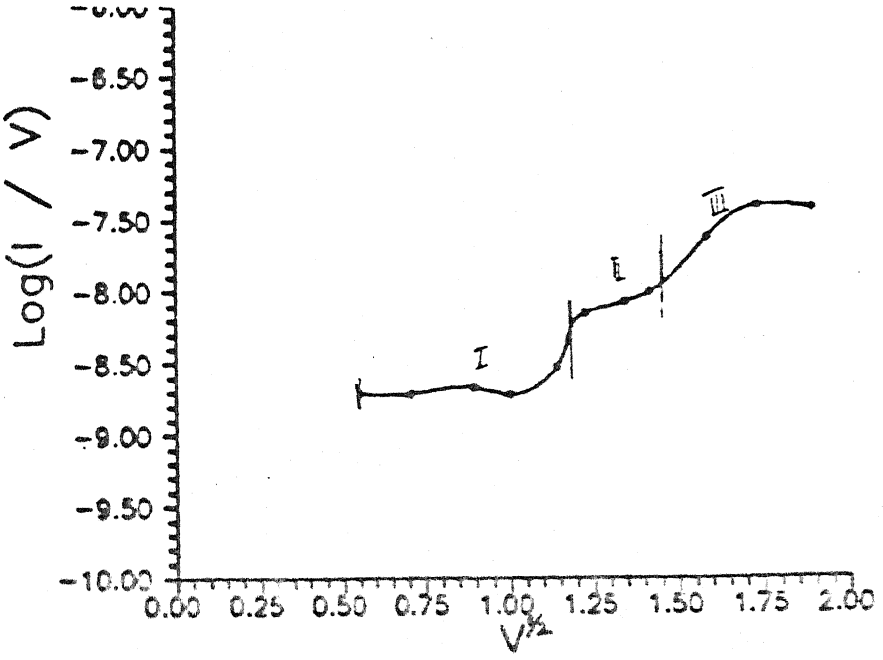
-6.50
-7.00
-7.50
-8.00
-8.50
-9.00
-9.50
-10.00
Log(I / V)
0.00 0.25 0.50 0.75 1.00 1.25 1.50 1.75 2.00
V^1/2
I
II
III

(c)

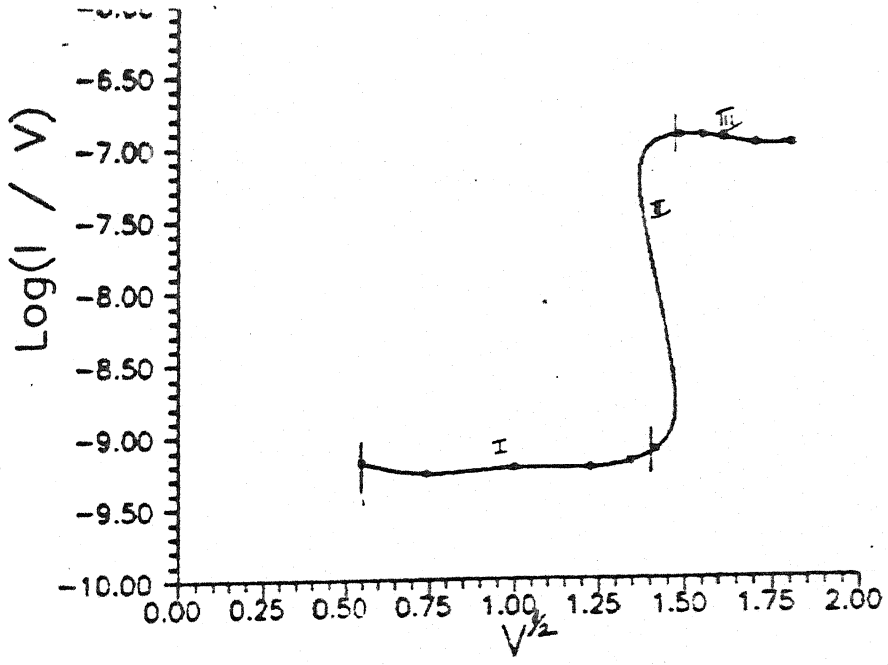
-6.50
-7.00
-7.50
-8.00
-8.50
-9.00
-9.50
-10.00
Log(I / V)
0.00 0.25 0.50 0.75 1.00 1.25 1.50 1.75 2.00
V^1/2
I
II
III

(d)

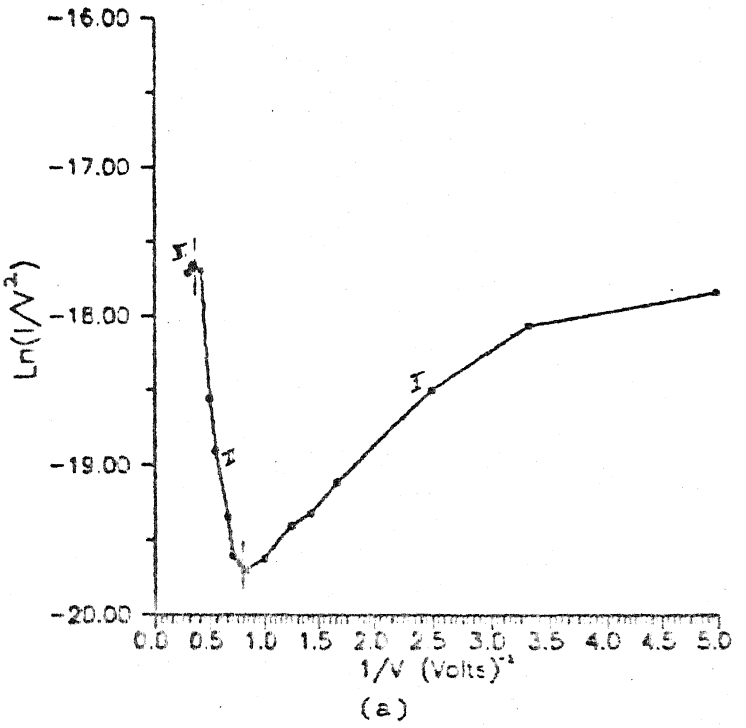

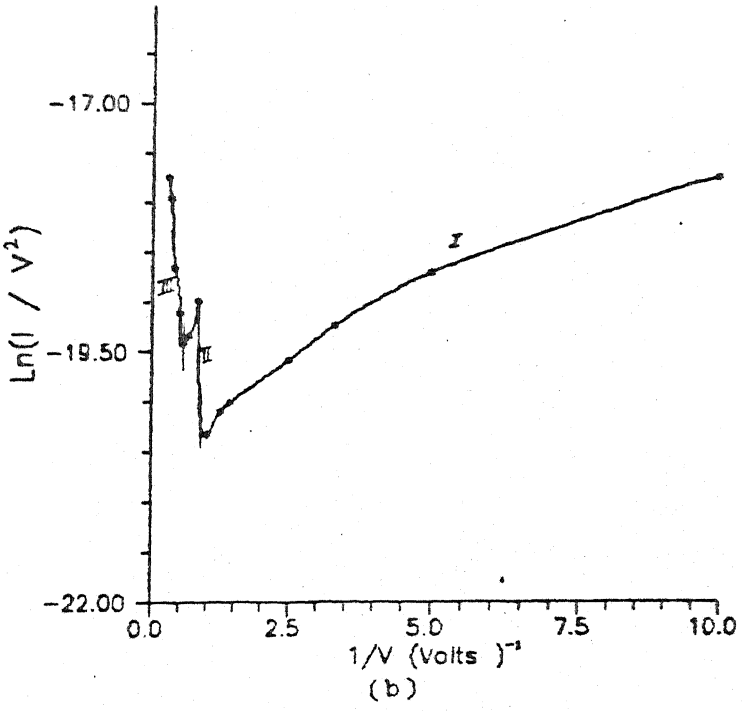

Fig.3.6 Ln (I / V) - 1 / V plots of Al-Al_2O_3-Al structure for insulator thickness (a) 3.8 nm (b) 4.4nm (c) 4.9 nm (d) 5.7 nm

continued . . .

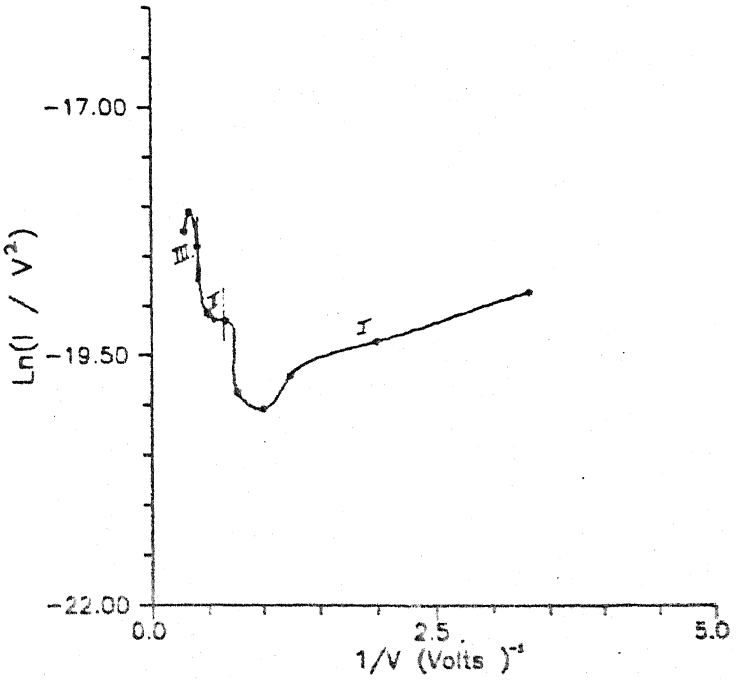
-17.00
-19.50
-22.00
Ln(I / V²)
0.0
2.5
5.0
1/V (Volts)⁻¹
III
II
I

(c)

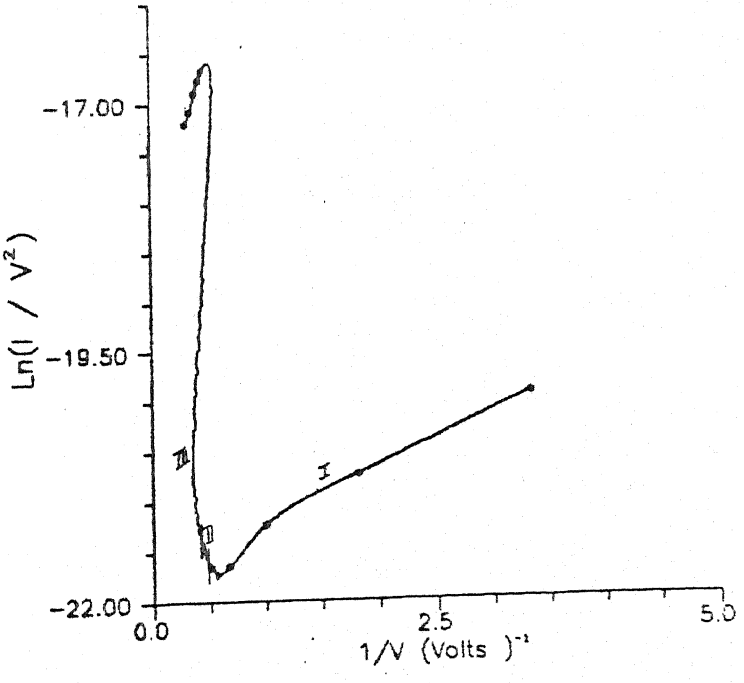
-17.00
-19.50
-22.00
Ln(I / V²)
0.0
2.5
5.0
1/V (Volts)⁻¹
III
II
I

(d)

TABLE 3.4 : CHARACTERISTICS OF VARIOUS CONDUCTION MODES FOR THIN INSULATING FILM

Conduction	Plot	Nature	Remarks
Ohmic	I vs V	Linear	Ohms Law
Space-Charge Limited	I vs V	Non-Linear	Childs Law[57]
	logI vs logV	Linear with slope 2 Linear with slope 3	Cube Law[54]
Tunneling	$\log(I/V^2)$ vs $1/V$	Straight line with negative slope	Fowler Nordhiem equation [6,27]
	logI vs $\sqrt{V}$	Straight line	Fowler Nordhiem equation plotted this way [96]
Schottky Emission	logI vs $\sqrt{V}$	Straight line with positive slope	Schottky Equation [12]
	$\log(I/V^2)$ vs $1/V$	Curve with a definite minimum	Modified Schottky equation [96,2]
Poole Frenkel Effect	logI vs $\sqrt{V}$	Straight line	Schottky Equation with $2\beta_s = \beta_{pf}$ [12]
	$\log(I/V)$ vs $\sqrt{V}$	Straight line Horizontal	Poole Frenkel Current expression [45]

Ohms Law: $I \propto V$

Childs Law: $I \propto V^2/t^3$ t : insulator thickness

Cube Law: $I \propto V^3$

Fowler Nordhiem equation: (Normal form) $I = A V^2 \exp(-A'/V)$ A,A' are constants

Schottky equation: Normal form $I = B \exp(B' \sqrt{V})$ B,B' are constants

Modified form $\ln(I/V^2) = B'' \sqrt{V} + 2 \ln(1/V)$ B'' is a constant

TABLE 3.5 : Different Parameters Determined for Al-Al_2O_3-Al Structure in Region I and its Sub-regions Ix and Iy (Fig. 3.4)

Region I			Region Ix		Region Iy				
Thickness Al_2O_3 t nm	Barrier height ϕ eV	β_s eV Expt.	Slope log I - log V	Voltage ranges volts	Slope of log I - log V	Voltage ranges volts	ϕ eV	β_s eV Expt.	β_s eV theor.
3.8	0.704	0.0205	0.42	0 - 0.71	1.36	0.71-1.21	0.753	0.0496	0.351
4.4	0.751	0.037	0.7	0 - 0.4	1.17	0.4-1.02	0.781	0.0976	0.326
4.9	0.744	0.042	1.008	0 - 1	3.92	1 - 1.41	0.807	0.183	0.309
5.7	0.761	0.03	0.95	0 - 1.5	2.03	1.5 - 2	0.812	0.074	0.286

meanings. The experimental values of β_s are about ten times lower than the theoretically estimated values. Also, β_s does not show any particular trend with the thickness. In the present case since Schottky emission is operating in conjunction with ohmic current, discrepancies mentioned above are natural. Hill [49] has observed that β_s is about three times smaller than the theoretically estimated values for Al_2O_3 films . This disparity might have been caused by errors in thickness measurements and in the value of high frequency dielectric constant for Al_2O_3 . In this voltage range the plots can be further subdivided into two regions Ix and Iy. This is done first for the log I- log V plots and then for the other plots. Log I-log V plots give slopes $n \leq 1$ in region Ix and $n>1$ in region Iy. These values suggest ohmic behaviour of the junction in region Ix and non-ohmic in region Iy. Assuming Schottky emission to be the dominant mechanism in region Iy values of β_s determined from the slope (along BC Fig.3.4) are given in Table 3.5. These values are now only 2 to 7 times smaller than the theoretically estimated values and thus Schottky emission is considered to be applicable in the entire region I. It is therefore believed that current is ohmic in the voltage range near the origin. At some voltage Schottky emission starts dominating the conduction process. Further, $\ln(I/V^2)$ - I/V plots exhibit a definite minimum providing evidence for the existence of Schottky emission [94-95]. When region III was analysed, as per Table 3.4, tests for Schottky and Poole - Frenkel alongwith tunneling were positive. Further the plot could not be divided into two sub-regions of different mechanisms as was possible in region I. Needless to mention that this is the criterion cited in the literature for their existence [43,47]. The β values calculated

meanings. The experimental values of β_s are about ten times lower than the theoretically estimated values. Also, β_s does not show any particular trend with the thickness. In the present case since Schottky emission is operating in conjunction with ohmic current, discrepancies mentioned above are natural. Hill [49] has observed that β_s is about three times smaller than the theoretically estimated values for Al_2O_3 films . This disparity might have been caused by errors in thickness measurements and in the value of high frequency dielectric constant for Al_2O_3 . In this voltage range the plots can be further subdivided into two regions Ix and Iy. This is done first for the log I- log V plots and then for the other plots. Log I-log V plots give slopes $n\leq1$ in region Ix and $n>1$ in region Iy. These values suggest ohmic behaviour of the junction in region Ix and non-ohmic in region Iy. Assuming Schottky emission to be the dominant mechanism in region Iy values of β_s determined from the slope (along BC Fig.3.4) are given in Table 3.5. These values are now only 2 to 7 times smaller than the theoretically estimated values and thus Schottky emission is considered to be applicable in the entire region I. It is therefore believed that current is ohmic in the voltage range near the origin. At some voltage Schottky emission starts dominating the conduction process. Further, $\ln(I/V^2)$ - I/V plots exhibit a definite minimum providing evidence for the existence of Schottky emission [94-95]. When region III was analysed, as per Table 3.4, tests for Schottky and Poole - Frenkel alongwith tunneling were positive. Further the plot could not be divided into two sub-regions of different mechanisms as was possible in region I. Needless to mention that this is the criterion cited in the literature for their existence [43,47]. The β values calculated

for Schottky emission and Poole-Frenkel effect are inconsistent with the theoretical values (see Table 3.6). The criteria used in the literature for the existence of Schottky emission and/or Poole-Frenkel effect as the conduction mechanism are the following : (i) agreement between theoretical determined values of β values from lnI vs $V^{\frac{1}{2}}$ plots and (ii) lowering in barrier height due to image force. There is considerable difference between β values obtained in region III of the ln I - $V^{\frac{1}{2}}$ plots and the theoretical values for various Al-Al_2O_3-Al structures. However, the experimentally determined barrier heights are significantly lower than the theoretical values (Table 3.6).A plot of Al_2O_3 thickness as a function of voltage for a given current exhibits nonlinearity (Fig.3.7) implying that the electrodes are rate limiting in the conduction process and there exists space-charge limited current as well [45]. The slopes of logI-logV plot in this region III were found to be greater than 2 providing evidence for the presence of voltage sensitive traps in Al_2O_3 (which is presumably in amorphous state) [18,41]. These traps once filled completely due to electron injection from the cathode will not limit the current further. Tests for tunneling turn out to be positive in region III as slope of $\ln(I/V^2)$ - I/V plots is negative [Fig 3.6]. In summary , we can say that traps are present in the amorphous Al_2O_3 layer and the conduction is mainly due to thermal field emission.In this process, an electron in the potential well of the trap is partly excited and then tunnels through the reduced barrier. Region II appears to be a transition zone in which conduction is governed by the mixture of all the mechanisms operating in region I & region III. The extent to which each mechanism contributes varies with the oxide thickness and nature of the individual sample.

ABLE 3.6 : The values of conduction coefficients (β_s & β_{pf}) determined in region III of an Al - Al_2O_3 - Al structure with insulator thickness (a) 3.8 nm (b) 4.4 nm (c) 4.9 nm (d) 5.7 nm

t (nm)	Expt. β_s eV	Expt. β_{Pf} eV	Theo. β_s eV	Theo. β_{Pf} eV
3.8	0.027	0.054	0.351	0.702
4.4	0.072	0.143	0.326	0.652
4.9	0.061	0.127	0.309	0.619
5.7	0.008	0.016	0.286	0.573

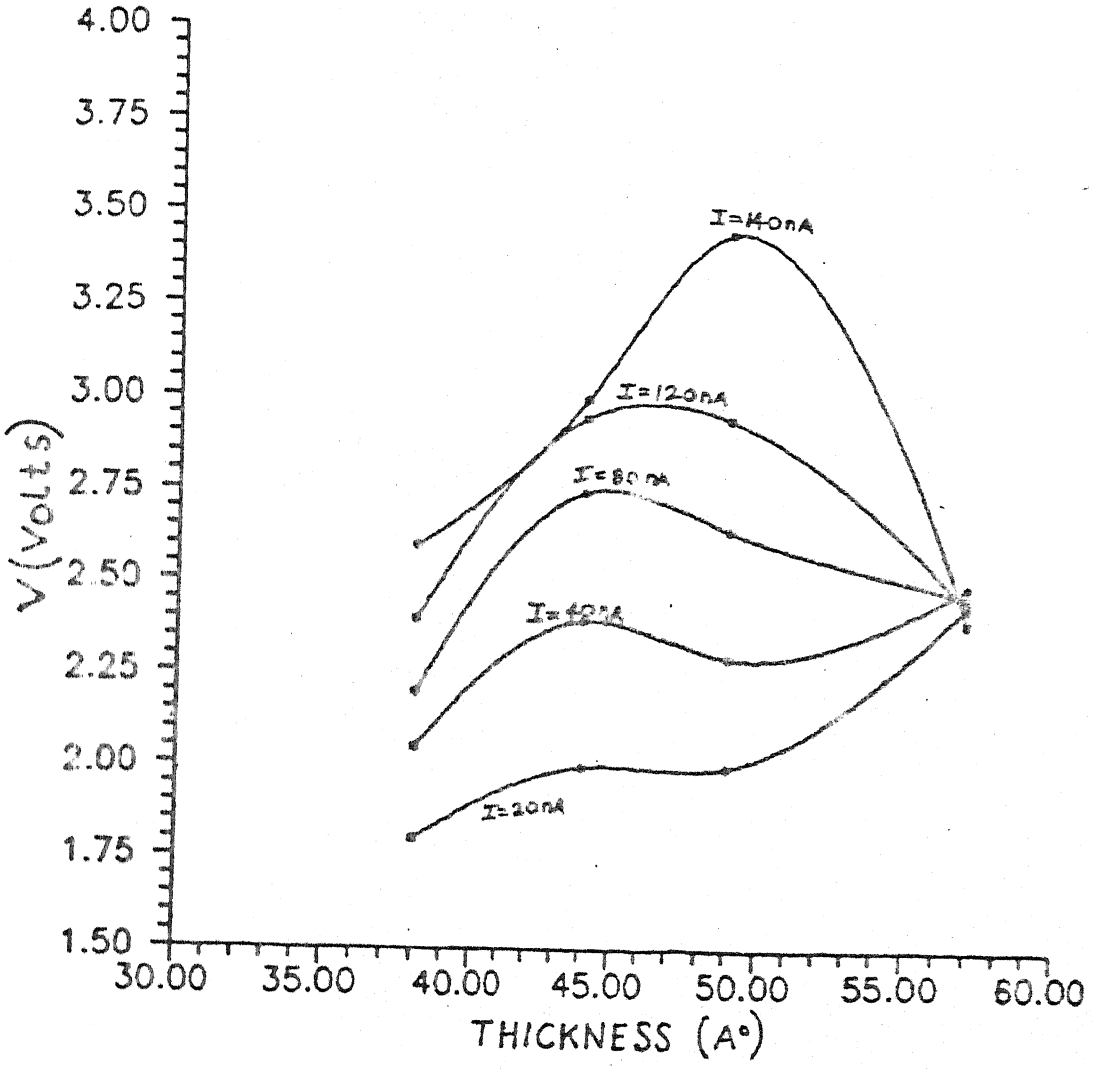

Fig 3.7 Voltage(V)-Thickness(tA°) curves for Al-Al_2O_3-Al structure at constant current I (a) 20 nA (b) 40 nA (c) 80 nA (d) 120 nA (e) 140 nA

ndentifying the conduction mechanism in thin Al_2O_3 films, on the basis of mechanisms reported in the literature lead to nconsistent results. i.e. While one test predicts the occurence of a particular mechanism, the other negates it . This indicates that there are no unique tests available for analysing different mechanisms. Therefore, all possible tests are performed with the data in the present investigation. Only those mechanisms which provided large number of positive tests are taken as the dominant process. The situation however becomes complex when various processes are simultaneously present. It then becomes difficult to determine the contribution of each mechanism. The experimental results presented above also indicate that in the lower voltage range the current is ohmic, Schottky emission and thermal field emission (modified Poole-Frenkel) types at the same time.

The I-V characteristics in region (a) are found to be reproducible even after a lapse of 24 hours (Fig.3.8]. This suggests that at low voltage no effective change in the properties of the dielectric layer takes place.

Al-Al_2O_3-Al junctions having insulating layer thickness between 3.8 and 4.4 nm show a monotonic rise in current with voltage in (b) region of the I-V characteristics (Fig.3.9 a,b). These observations are different from those prevailing in samples with thicker dielectric layers (discussed later)because no decrease in current or appearance of negative resistance region is seen. The continous rise in current can be explained on the basis of avalanche breakdown mechanisms & emergence of discontinuities in Al_2O_3. The conducting electrons, accelerated due to applied electric field create more electrons on collision. This

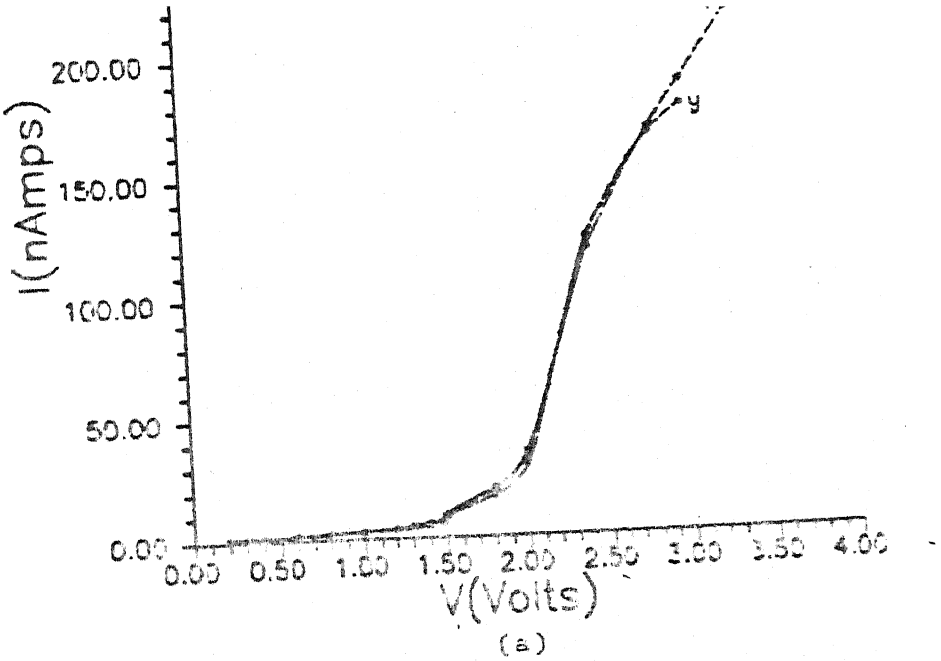

(a)

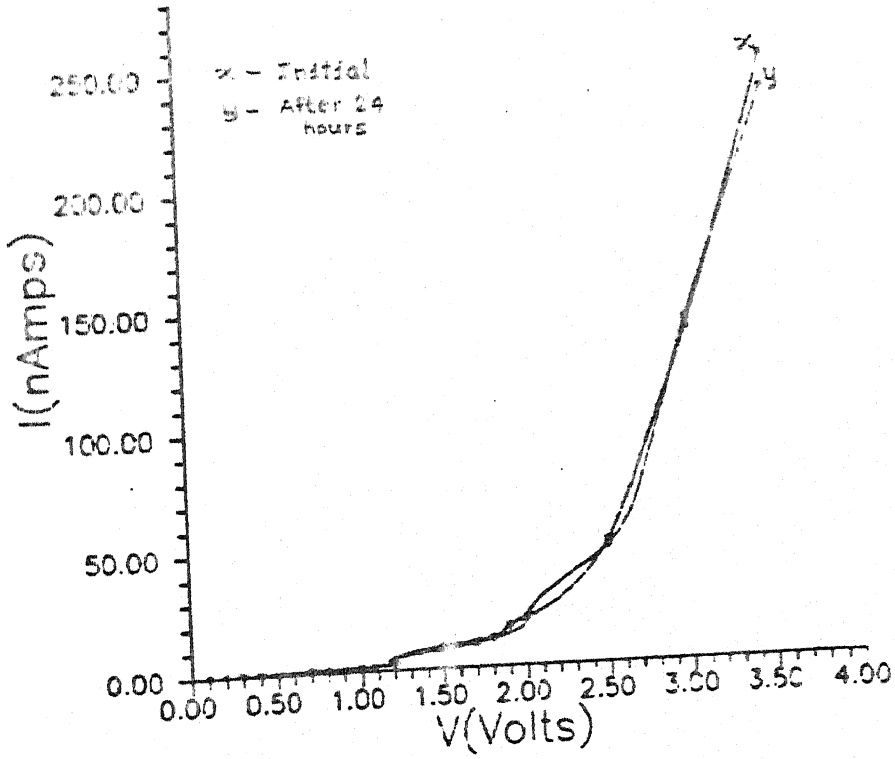

(b)

Fig.3.8 I - V characteristics for Al-Al_2O_3-Al structure taken initially and after 24 hours for insulator thickness (a) 3.8 nm (b) 4.4 nm (c) 4.9 nm (d) 5.7 nm

continued . . .

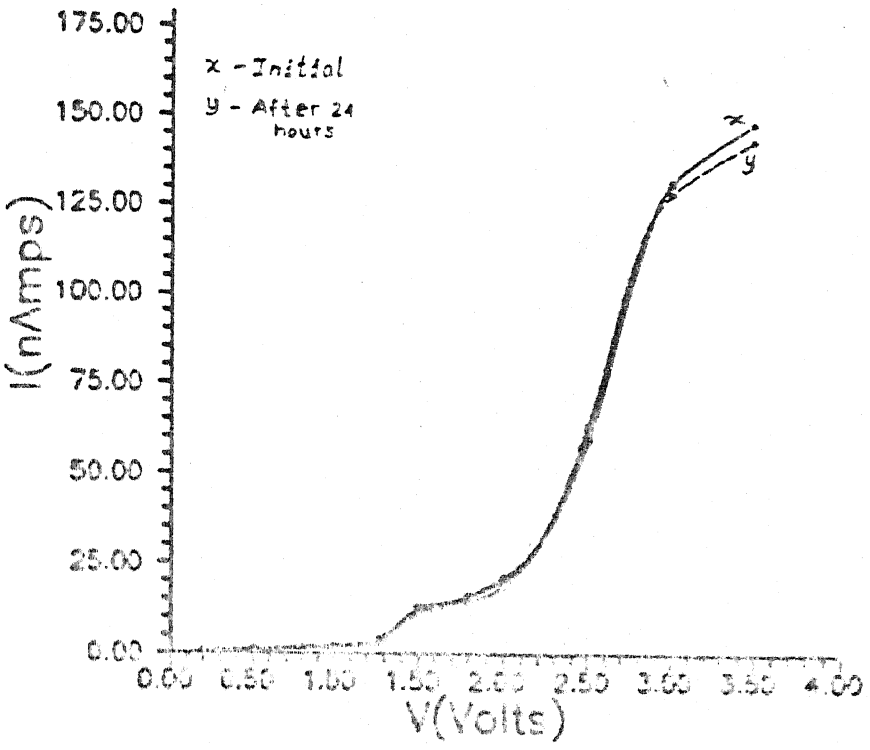
x - Initial
y - After 24 hours
I(nAmps)
V(Volts)
175.00
150.00
125.00
100.00
75.00
50.00
25.00
0.00
0.00
0.50
1.00
1.50
2.00
2.50
3.00
3.50
4.00

(c)

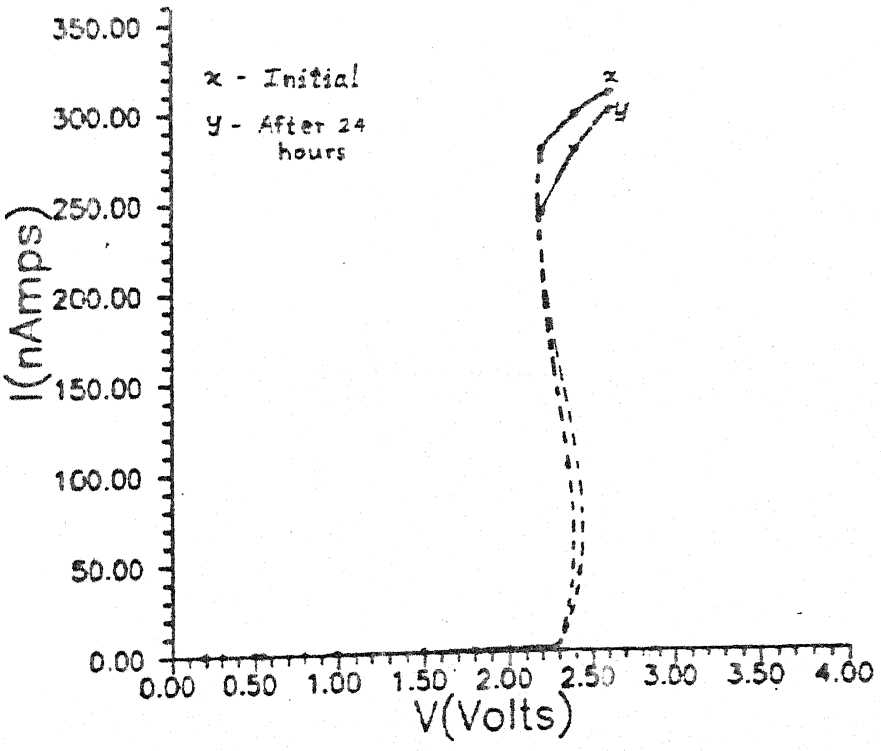
x - Initial
y - After 24 hours
I(nAmps)
V(Volts)
350.00
300.00
250.00
200.00
150.00
100.00
50.00
0.00
0.00
0.50
1.00
1.50
2.00
2.50
3.00
3.50
4.00

(d)

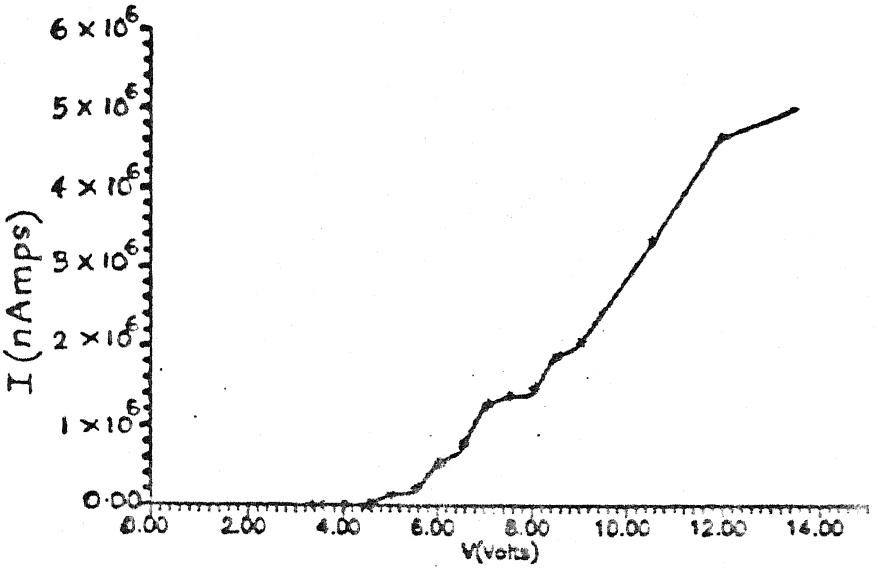

(a)

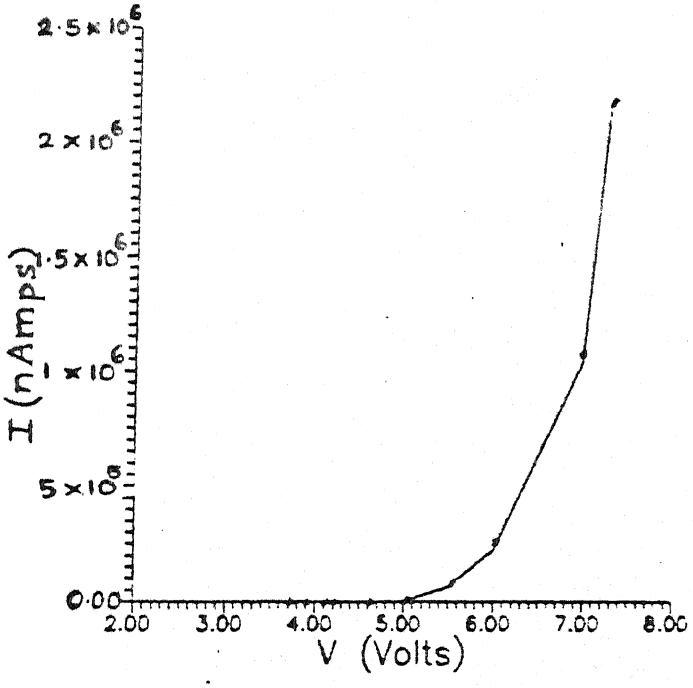

(b)

Fig.3.9 I - V characteristics of Al - Al_2O_3 - Al structure in category b and c for insulator thickness (a) 3.8nm (b) 4.4nm (c) 4.9nm (d) 5.7nm

continued . . .

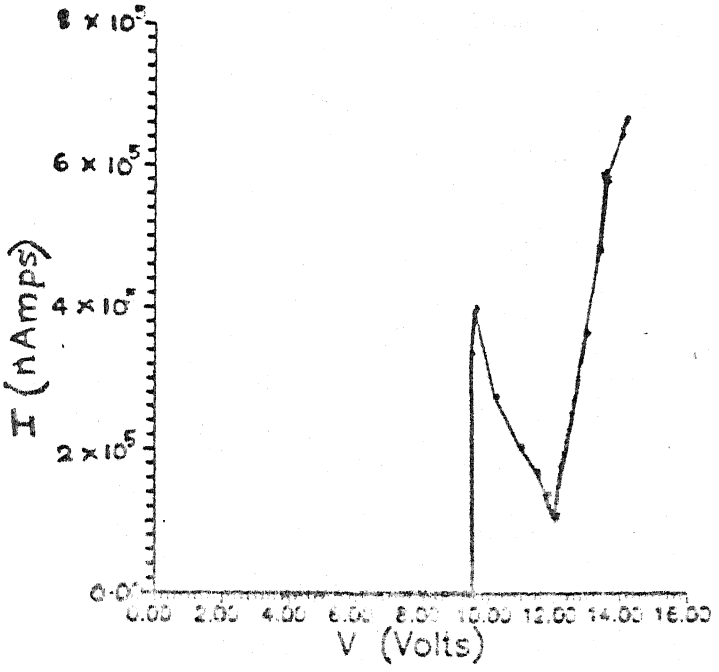
I (nAmps)
V (Volts)
0.00
2.00
4.00
6.00
8.00
10.00
12.00
14.00
16.00

(c)

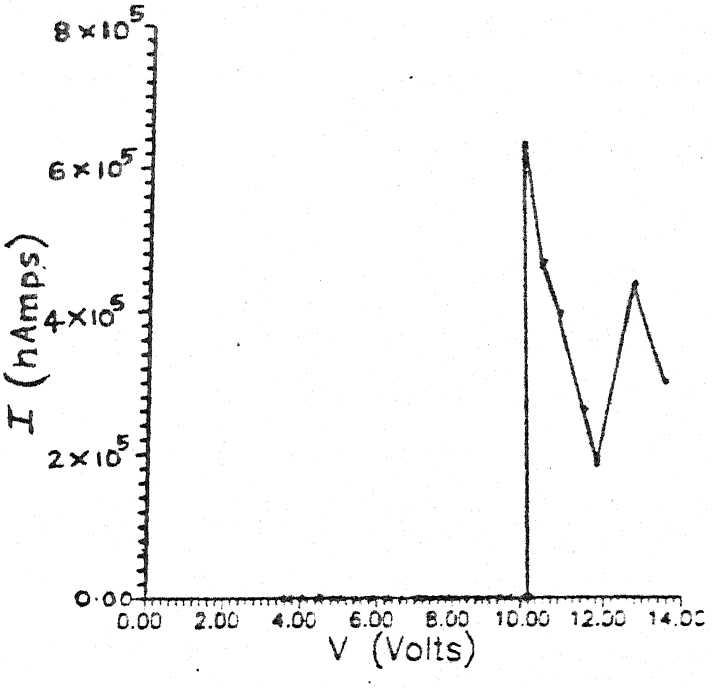
8×10^5
6×10^5
4×10^5
2×10^5
0·00
I (hAmps)
0.00
2.00
4.00
6.00
8.00
10.00
12.00
14.00
V (Volts)

(d)

irreversible process leads to loss of aluminium - Al_2O_3 contact. This has become evident from the fact that no current is observed through the Al_2O_3 film after a lapse of 24 hours. For Al_2O_3 films of thicknesses 4.9 and 5.7 nm in the second region(b), the current first increases upto a certain voltage after which it gives rise to a differential negative resistance region (Fig.3.9c and d). This increase in current in region (b) is attributed to the 'Forming' process. In Al-Al_2O_3-Al systems, forming process and negative resistance have been reported for anodic and r.f. sputtered Al_2O_3 films only [45,56,57]. The presence of these effects in thermally grown alumina as well suggests that the nature of Al_2O_3 layer is quite similar and the phenomena is basically the property of Al_2O_3 itself. The forming process leads to a radical and essential permanent change in the electrical properties of the insulating film. The voltage at which maximum current is observed in the forming region is called the 'Forming' potential V_F. This parameter is found to be nearly the same for the two oxide thicknesses 4.9 nm & 5.7 nm , implying that 'Forming' is a voltage controlled process. Various models have been put forward to explain the occurence of forming and the observed VCNR effect. But the appearance of negative resistance region and fluctuations in current with voltage can be better explained by filamentary model as proposed by Dearnaley et al [15]. According to this model there exists high electric field at the irregularities, present near the cathode surface. This leads to micro-structural changes and the emergence of conducting filaments. The electric field at the tip of the filament is unusually high and so it helps in the growth of the conducting filaments and in joining them. Thus a conducting link is established eventually, between the electrodes. Also,

since the forming potential is independent of Al_2O_3 thickness filaments are supposedly initiated in well-localised regions [15,45,96]. Wherever the field takes a high value these localised channel allow electrical conduction , leaving rest of the volume intact as dielectric. As a consequence, numerous narrow regions of high conductivity emerge in the formed insulating film. However the filaments are not uniform and have weak spots that determine their resistance. These are subjected to Joule heating. Associating a local temperature (T) with each filament, rupture may occur if T exceeds some maximum temperature T_{max}. Also, electrons suffer phonon scattering particularly at weak and hot spots of the filament. Both these account for the decrease in current with increase in voltage, i.e. appearance of negative resistance. Rise in current with applied voltage after reaching a minimum (fig.3.9 c,d) is observed again as the new filament channels emerge in due course in some other parts of the Al_2O_3. This processes may go on for a number of cycles. In fact, for Al_2O_3 of thickness 5.7 nm, another negative resistance region is observed and can be attributed to the process of rupturing of secondary filaments. The observations of fluctuations are also providing evidence for initiation of the dielectric breakdown process [55]. Eventually the entire Al_2O_3 film loses its insulating properties. There is a possibility of loss of contact of the electrode with Al_2O_3 at the interface. This amounts to the failure of the Al-Al_2O_3-Al device/junction. To check this, the current-voltage characteristics,of samples exhibiting forming, negative resistance and fluctuations in current has been observed after 24 hours. No current is observed to flow through the junction showing that dielectric breakdown of Al_2O_3 film has occured with or without loss

of electrode-Al_2O_3 contact.

3.3 Asymmetric nature of barrier

Al-Al_2O_3-Al devices have the same electrodes on both sides of the dielectric. Hence the barriers at the two interfaces is expected to be symmetric in nature. However, junctions prepared by thermal oxidation of aluminium and subsequent deposition of cross aluminium electrode are known to yield asymmetric barriers. So, values of barrier heights differ on both the interfaces. The reported values vary widely and lies between 0.7 eV- 1.8eV [6,23,28,36]. Nevertheless, the barrier height is invariably found to be smaller for the bottom electrode (on which aluminium oxide is grown) in comparison to the top one. In order to check the asymmetry nature of the barrier, current-voltage characteristics have been recorded by making base electrode negative in one case while positive in the other. Fig 3.10 shows the I-V characteristics in both the situations for a 3.6 nm thick Al_2O_3 film. It is seen that in the entire voltage range the current is higher when the base is negative than when it is positive. Also, the experimentally determined values of barrier height are 0.67 eV and 0.7 ev for bottom and top electrode respectively. This difference is explained by assuming the graded type barrier at the interface between the bottom electrode and oxide.This graded type barrier is supposed to be caused by migration of aluminium ions into the oxide during oxidation process [20].However, the barrier is abrupt at the interface between top aluminium layer and the oxide as the deposition of top electrode is made after the oxide formation. In fact the graded junction can be semiconducting even having an n-type transition zone (Fig.3.11) [19]. We see from

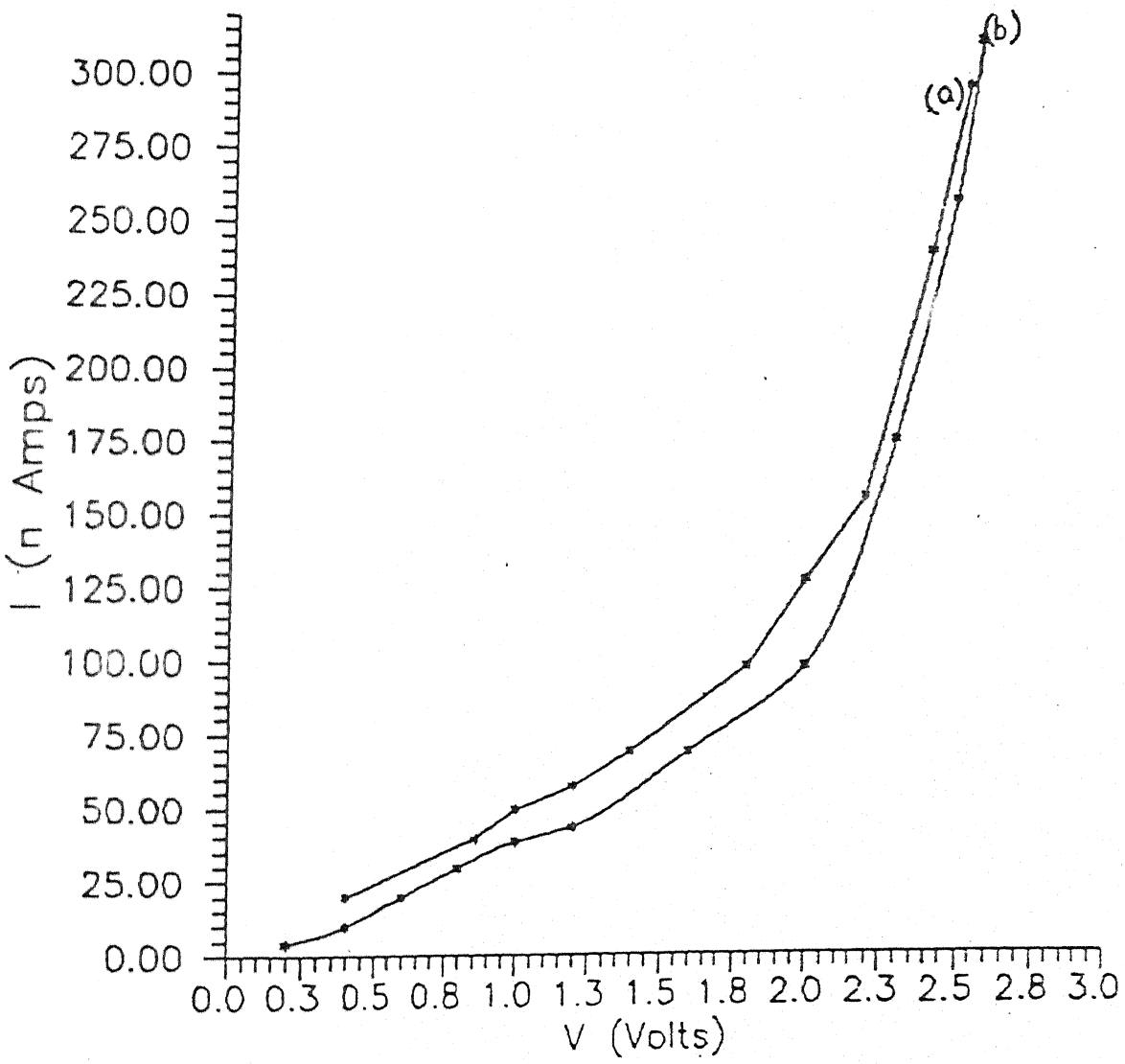

Fig.3.10 I - V characteristics of an 3.6 nm thick Al_2O_3 film with (a) base negative (b) base positive

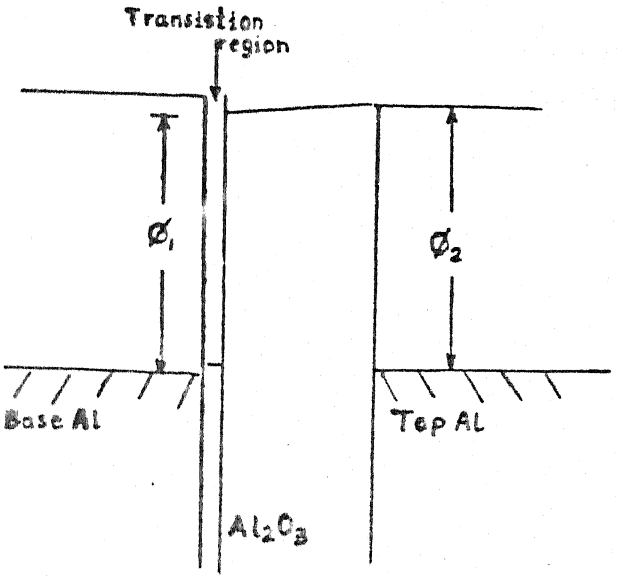

(a)

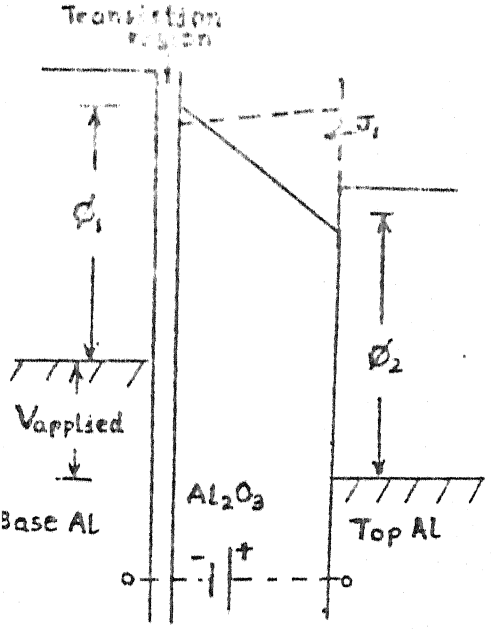

(b)

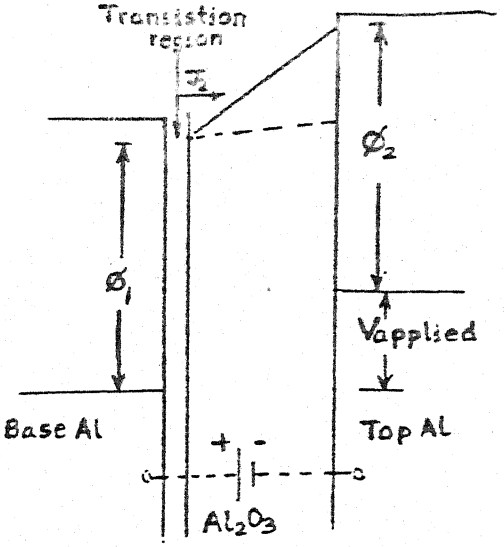

(c)

Fig.3.11 Idealised trapezoidal potential barrier showing barrier shapes in Al-Al_2O_3-Al structures (a) unbiased (b) base aluminium electrode negatively biased (c) base aluminium electrode positively biased

Fig.3.11 that with base negative (assuming conduction due to electrons drifting in a direction opposite to thr electric field), the electrons will flow `downhill' the barrier giving current J_1 but with base positive the electrons have got to 'climb' up the barrier and so will encounter resistance. This may in the process lead to scattering and collision of electrons which impedes the flow, resulting in currrent J_2, smaller than J_1.

CHAPTER 4

CONCLUSIONS

a) Al-Al_2O_3-Al devices/junctions have been fabricated by thermal oxidation of aluminium with dielectric thickness ranging from 4-6 nm. In the low voltage range (< 3V) their I - V characteristics exhibit three distinct regions. In the first region near the origin, the current is very low and samples show nearly ohmic behaviour because of the high resistance of the dielectric. The second mechanism in this region is Schottky emission. The third region (1.5V - 3V) involves thermal-field emission alongwith the space charge limited current. The second region corresponds to a transition zone where all the above conduction mechanisms operate simultaneously with unknown degree of dominance.

b) The barrier height corresponding to Schottky emission regime increases with oxide thickness. However,the experimental values are smaller than the theoretically estimated values. This is presumably due to reduction of barrier itself following the interaction of image forces with the applied electric field.

a) The existence of `Forming' process involving perceptible change in dielectric properties followed by voltage controlled negative resistance (VCNR) has been observed for the first time in junctions with thermally grown Al_2O_3 layers of thickness in excess of 5nm.'Forming' potential for Al-Al_2O_3-Al is about 10V and is independent of dielectric thickness. Forming and VCNR

can be understood by the formation of channels of conducting filaments in Al_2O_3 and their rupture due to joule heating, respectively. The dielectric breakdown of Al_2O_3 occurs beyond the VCNR regime.

b) Al-Al_2O_3-Al junctions with thinner oxide layers (<5nm) show continous rise in current without any `Forming' or VCNR region. The steep rise in current is responsible for its eventual failure.

c) The emergence of discontinuties, possible loss of electrode-oxide contact and/or total destruction of the oxide layer appears to be responsible for the dielectric breakdown of the Al-Al_2O_3-Al junctions.

a) The electrode-oxide interface exhibits asymmetry in the sense that current through the junction is more when the base electrode (on which aluminium oxide is thermally grown) is negative than when it is positive. This indicates the asymmetric nature of potential barrier between the metal and Al_2O_3.

b) The barrier at the base electrode - oxide interface appears to be graded type and is formed due to migration of aluminium ions into the oxide. However, the barrier at the interface between the top metal and the oxide appears to be more or less abrupt in nature.

REFERENCES

1. Frenkel J. Phys. Rev. 36(1930)1604
2. Murphy E. and Good R.H. Jr. Phys. Rev. 102(1956)1464.
3. Holm R. J. Appl. Phys. 22(1951)569
4. Stratton R. J. Appl. Phys. and Chem. of Solids 23(1962)1177
5. Pollack S.R. and Morris C.E. J. Appl. Phys. 35(1964)1503
6. Simmons J.G. J. Appl. Phys. 34(1963)2581
7. Vodenicharov H.M. and Christov S.G. Solid state electronics 15(1972)933
8. Kanter H. and Feibelman W.A. J. Appl. Phys. 33(1962)3580
9. Geppert D.V. J. Appl. Phys. 34(1963)490
10. Mead C.A. J.Appl.Phys. 32(1962)646
11. Lamb D.R. " Electrical conductions mechanisms in thin insulating films" Methuen and Company Ltd. 1967
12. Maissel L.I. and Glang R. " Handbook of thin film technology" Mcgraw Hill Book Company 1970
13. Abraham E. and Miller A. Phys. Rev. 120(1960)745
14. Mycielski J. Phys. Rev. 123(1961)1
15. Dearnaley G., Stoneham A.H. and Morgan D.V. Reports of Progress in Physics 33(1970)1129
16. Simmons J.G. Transactions of Metallurgical Society of AIME 233(1965)485
17. Simmons J.G. J. Appl. Phys. 34(1963)1793
18. Geppert D.V. J. Appl. Phys. 33(1962)2993
19. Simmons J.G. J. Appl. Phys. 35(1964)2472
20. Pollack S.R. and Morris C.E. J. Appl. Phys. 35(1964)1503
21. Handy R.M. Phys. Rev. 126(1962)1968

22. Gundlach K.H. J. Appl. Phys. 44(1973)5005

23. Gundlach K.H. and Holzl Surface Science 27(1971)125

24. Kumagai Y., Inukai K. and Suzuki Y. J. Appl. Phys. 42(1971)2981

25. Wintle H.J. J. Appl. Phys. 44(1973)2514

26. Gupta H.M. and Overstraeten R.J.von J. Appl. Phys. 46(1975)2675

27. Srivastava P.C., Bardhan A.R. and Bhattacharya D.L. Int. J. of Electronics 46(1979)547

28. Sarnot S.L. and Dubey P.K. Solid State Electronics 15(1972)745

29. Giaver I. and Fisher J.C. J. Appl. Phys. 32(1961)172

30. Giaver I. and Megerle K. Phys. Rev. 122(1961)1101

31. Blackford B.L. and March R.H. Canadian J. of Phys. 46(1968)141

32. Douglass D.H. and Meservy R. Phys. Rev. 135(1964)A19

33. Giaver I. , Hart H.R. Jr. and Megerle K. Phys. Rev. 126(1962)941

34. Simmons J.G. Phys. Rev. Lett. 15(1965)967

35. Emptage P.R. and Tantraporn W. Phys. Rev. Lett. 8(1962)267

36. Arya S.P.S. and H.P.Singh Thin Solid Films 91(1982)

37. Hartman T.E. J. Appl. Phys. 35(1964)3283

38. Pollack S.R. and Morris C.E. Trans. of Meta. Soc. of AIME 233(1965)497

39. Chang L.L. Stiles L. Stiles P.J. J. Appl. Phys.38(1967)4440

40. Schmidt P.F. et al J. Appl. Phys. Chem. of Solids 15(1960)270

41. Vodenicharov H.M. and Christov S.G. Phys. Stat. Sol.(a) 25(1974)387

42. Pollack S.R. J. Appl. Phys. 34(1963)877

43. Simmons J.G. Phys. Rev. 155(1967)657

44. Mead C.A. Phys. Rev. 128(1962)2088

45. Ray A.K. and Hogarth C.A. Int. J. of Elect. 57(1984)1

46. Hirose H. and Wada Y. Jap. J. of Appl. Phys. 4(1965)639

47. Nazar F.M. and Atiq M.T. Int. J. of Elect. 47(1979)81

48. Johansen I.T. J. Appl. Phys. 37(1966)499

49. Hill R.M. Phil. Mag. 23(1971)59

50. Antula J. Phys. Stat. Sol. 24(1967)89

51. Mott N.F. and Gurney R.W. " Electronic processes in Ionic Crystals" 2ded Oxford University Press 1948 chap

52. Rose A. Phys. Rev. 97(1955)1538

53. Lampert M.A. Phys. Rev. 103(1956)1648

54. Lampert M.A. Phys. Rev. 125(1962)126

55. Pulfrey D. L. and Shousha A.H.M. J. Appl. Phys. 41(1970)2838

56. Rahman A. and Raven M.S. Thin Solid Films 71(1980)7

57. Hickmott T.W. J. Appl. Phys. 32(1962)2669

58. Hickmott T.W. Thin Solid Films 9(1972)431

59. Collins R.A., Bowman G. and Sutherland R.R. J. Phys. D 4(1971)L49

60. Simmons J.G. and Verderber R.R. Proc. of Roy. Soc. A301(1967)77

61. Khan M.N. , Khan M.I. and Hogarth C.A. Phys. Stat. Sol. (a) 61(1980)251

62. Kuriki S.,Noya A. and Matsumoto G. Thin Solid Films 48(1978)27

63. Tanaka K.,Vemura Y. and Owata M. Thin Solid Films 50(1978)L25

64. Hickmott T.W. J. Appl. Phys. 35(1964)2679

65. Dearnaley G. Phys. Lett. 25A(1967)760

66. Barriac C., Pinnard P. and Davoine F. Phys. Stat. Sol. 34(1969)621

67. Greene P.D., Bush E.L. and Rawlings I.R. Proc. Symp. on deposited thin film dielectric materials , Montreal 1968 , Ed. F. Vratny (N.Y. The Electrochemical Society, 1969) P167-85

68. Beidermann H. Thin Solid Films 18(1973)39

69. Emmer I. Thin Solid Films 20(1974)43

70. Kanter H. and Feibelman W.A. J. Appl. Phys. 33(1962)3580

71. Klein N. and Gafni H. IEEE Trans. Electron Devices ED13(1966)281

72. Klein N. and Levanon N. J. Appl. Phys. 38(1967)3721

73. Gould R. D. and Hogarth C.A. Int. J. Elect. 37(1974)157

74. O'Dwyer J.J. J. Appl. Phys. 40(1969)3887

75. Seitz F. Phys. Rev. 76(1949)1376

76. O'Dwyer J.J. "The theory of electrical conduction and breakdown in solid dielectrics" Clarendon Press, Oxford 1973

77. Rose R.M.,Shepard L.A.,Wulff J. "The structure and properties of materials,Volume ,Electronic properties " Wiley Eastern Limited 1987 pg253

78. Shousha A.H.M.,Pulfrey and Young L. J. Appl. Phys. 43(1972)15

79. Ridley B.K. J. Appl. Phys. 46(1975)998

80. Budenstein P.P. IEEE Trans. Electr. Insul. 15(1980)225

81. Klein N. Thin Solid Films 100(1983)335

82. Svensson C. and Shumka A. Int. J. Electron. 38(1975)69

83. Wijenberg H.J. de Wit ch. and Crevecoeur C. J. Electrchem. Soc. 123(1976)1479

84. Young L. "Anodic oxide films," Academic Press, New York 1961

85. Filby J.D. and Nielson S. J. Electrochem. Soc. 112(1965)957

86. Spratt J.P. , Schawrz R.F. and Kane W.M. Phys. Rev. 6(1961)341

87. Meyerhoffer D. and Ochs S.A. J. Appl. Phys. 34(1963)2535

88. Argall F. and Jonscher A.K. Thin Solid Films 2(1968)185

89. Mead C.A. Phys. Rev. Lett. 6(1961)545

90. Ku H. Y. and Ullman F.G. J. Appl. Phys. 32(1964)265

91. Simmons J.G. Appl. Phys. Lett. 6(1965)54

92. Hebard A.F., Ajuria S.A. and Eick R.H. Appl. Phys. Lett. 51(1987)1349

93. Lawless K.R. Rep. Prog. Phys. 37(1974)231

94. Harris L.A. J. Appl. Phys. 35(1964)268

95. Bardhan A.R., Srivastava P.C., Chatterjee A.,, Bhattacharya D.L. Int. J. Electron.40(1976)313

96. Dearnaley G. Morgan D.V. and Stoneham A.M. J. Non-cryst. Solids 4(1970)593

97. Das V.D. and Jagadeesh M.S. Phys. Stat. Sol.(a) 66(1981)327